AD-A083 338 LOCKHEED MISSILES AND SPACE CO INC PALO ALTO CA PALO --ETC F/6 20/11
DYNAMIC INSTABILITY OF AN ELASTIC CYLINDRICAL SHELL EXCITED BY --ETC(U)
JUL 79 T L GEERS, C L YEN DNA001-78-C-0029
UNCLASSIFIED LMSC/D676760 DNA-5026Z NL

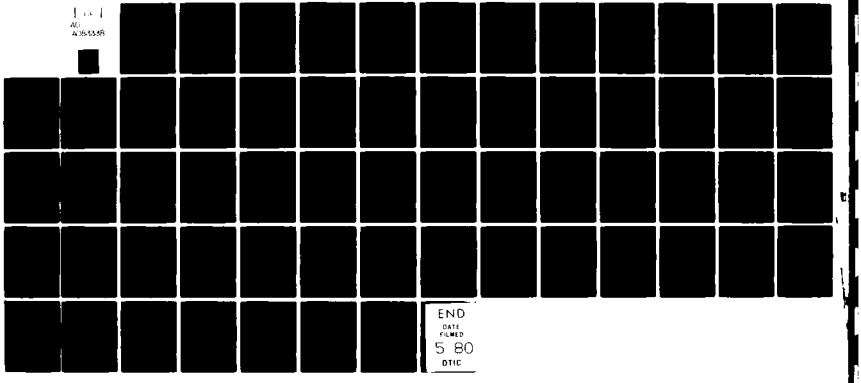

END
DATE FILMED
5 80
DTIC

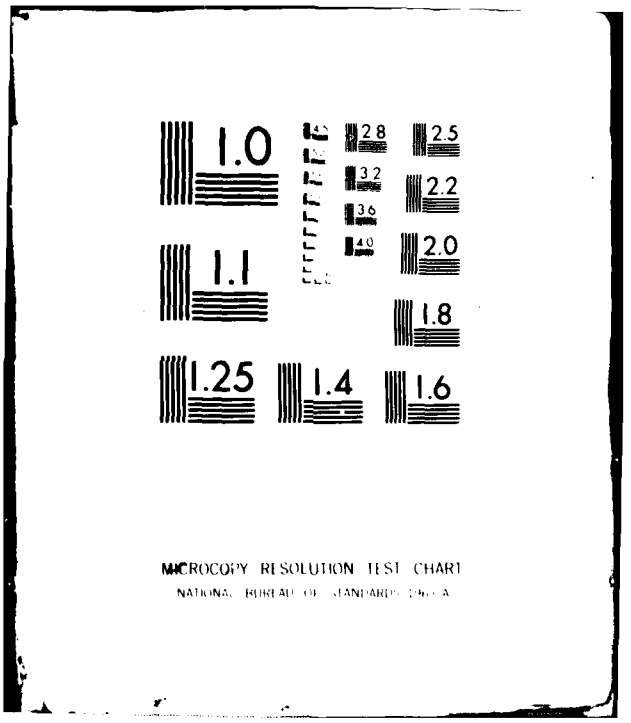
1.0
1.1
1.25
1.4
1.6
1.8
2.0
2.2
2.5
2.8
3.2
3.6
4.0
MICROCOPY RESOLUTION TEST CHART
NATIONAL BUREAU OF STANDARDS-1963-A

DNA 5026Z

DYNAMIC INSTABILITY OF AN ELASTIC CYLINDRICAL SHELL EXCITED BY A TRANSIENT ACOUSTIC WAVE

Lockheed Palo Alto Research Laboratory
3251 Hanover Street
Palo Alto, California 94304

12 July 1979

Interim Report for Period 14 November 1977—12 July 1979

CONTRACT No. DNA 001-78-C-0029

APPROVED FOR PUBLIC RELEASE;
DISTRIBUTION UNLIMITED.

THIS WORK SPONSORED BY THE DEFENSE NUCLEAR AGENCY
UNDER RDT&E RMSS CODE B344079464 Y99QAXSF50120 H2590D.

Prepared for
Director
DEFENSE NUCLEAR AGENCY
Washington, D. C. 20305

Destroy this report when it is no longer needed. Do not return to sender.

PLEASE NOTIFY THE DEFENSE NUCLEAR AGENCY, ATTN: STTI, WASHINGTON, D.C. 20305, IF YOUR ADDRESS IS INCORRECT, IF YOU WISH TO BE DELETED FROM THE DISTRIBUTION LIST, OR IF THE ADDRESSEE IS NO LONGER EMPLOYED BY YOUR ORGANIZATION.

UNCLASSIFIED

SECURITY CLASSIFICATION OF THIS PAGE *(When Data Entered)*

REPORT DOCUMENTATION PAGE		READ INSTRUCTIONS BEFORE COMPLETING FORM
1. REPORT NUMBER DNA 5026Z	2. GOVT ACCESSION NO. AD-A083 338	3. RECIPIENT'S CATALOG NUMBER
4. TITLE *(and Subtitle)* DYNAMIC INSTABILITY OF AN ELASTIC CYLINDRICAL SHELL EXCITED BY A TRANSIENT ACOUSTIC WAVE		5. TYPE OF REPORT & PERIOD COVERED Interim Report for Period 14 Nov 77—12 Jul 79
		6. PERFORMING ORG. REPORT NUMBER LMSC-D676760
7. AUTHOR(s) T. L. Geers C. L. Yen		8. CONTRACT OR GRANT NUMBER(s) DNA 001-78-C-0029 new
9. PERFORMING ORGANIZATION NAME AND ADDRESS Lockheed Palo Alto Research Laboratory 3251 Hanover Street Palo Alto, California 94304		10. PROGRAM ELEMENT, PROJECT, TASK AREA & WORK UNIT NUMBERS Subtask Y99QAXSF501-20
11. CONTROLLING OFFICE NAME AND ADDRESS Director Defense Nuclear Agency Washington, D.C. 20305		12. REPORT DATE 12 July 1979
		13. NUMBER OF PAGES 62
14. MONITORING AGENCY NAME & ADDRESS*(if different from Controlling Office)*		15. SECURITY CLASS *(of this report)* UNCLASSIFIED
		15a. DECLASSIFICATION/DOWNGRADING SCHEDULE

16. DISTRIBUTION STATEMENT *(of this Report)*

Approved for public release; distribution unlimited.

17. DISTRIBUTION STATEMENT *(of the abstract entered in Block 20, if different from Report)*

18. SUPPLEMENTARY NOTES

This work sponsored by the Defense Nuclear Agency under RDT&E RMSS Code B344079464 Y99QAXSF50120 H2590D.

19. KEY WORDS *(Continue on reverse side if necessary and identify by block number)*

Fluid-structure Interaction
Dynamic Instability
Transient Shell Response

20. ABSTRACT *(Continue on reverse side if necessary and identify by block number)*

Governing equations are developed for the dynamic instability of an infinite, elastic, circular cylindrical shell submerged in an infinite fluid medium and excited by a transverse, transient acoustic wave. These equations derive from circumferential Fourier series decomposition of the field quantities appearing in appropriate energy functionals, and from application of the "residual potential formulation" for rigorous treatment of the fluid-structure interaction. Extensive numerical results are presented that provide

DD FORM 1 JAN 73 1473 EDITION OF 1 NOV 65 IS OBSOLETE

UNCLASSIFIED

SECURITY CLASSIFICATION OF THIS PAGE *(When Data Entered)*

20. ABSTRACT (Continued)

understanding of the phenomenology involved and permit evaluation of the "doubly asymptotic approximation" for treatment of the fluid-structure interaction.

PREFACE

The authors express their appreciation to their colleagues B. O. Almroth, F. A. Brogan and P. G. Underwood for their valuable suggestions regarding both theoretical and computational aspects of this study. Additional thanks are due Dr. Nicholas Basdekas of the Office of Naval Research for Sharing his knowledge of the literature.

TABLE OF CONTENTS

LIST OF ILLUSTRATIONS

LIST OF ILLUSTRATIONS (continued)

SECTION 1

INTRODUCTION

Although the literature is replete with analytical studies of the linear dynamic response of submerged structures, the dynamic instability of such structures has received relatively little attention [1]. In 1965, Di Maggio [2] studied the unstable dynamic response of an infinite flat plate with a sinusoidal imperfection in one direction subjected to an in-plane static loading in that same direction; the plate was suddenly released so as to interact with an acoustic medium on one side of the plate. He found that, in the vast majority of cases, the acoustic medium may be treated in the incompressible approximation. In 1972, Deng and Popelar [3] studied the parametric instability of a submerged cylindrical shell initially undergoing sinusoidal breathing motions. They also found that the acoustic medium could be accurately treated as imcompressible. References [4-6] report analyses of dynamically excited, submerged shells that exhibit instability characteristics. In all of these, however, approximate treatments of the fluid-structure interaction are used, which raises questions regarding the accuracy of the results.

This report presents a rigorous treatment of the dynamic instability of an infinite, elastic, circular cylindrical shell excited by a transverse, transient acoustic wave. The field quantities appearing in appropriate kinetic-energy, potential-energy, and work-potential functionals are expanded in circumferential Fourier series, and high-order terms are eliminated in a consistent manner. The residual potential formulation [7-9], which constitutes an exact formulation, is used to treat the fluid-structure interaction. The resulting modal response equations provide a complete and rigorous description of the dynamic processes.

The modal response equations are integrated numerically in time for excitation by plane waves of rectangular and exponential pressure-profile. Transient response histories are provided that portray: 1) modal response as a function of incident-wave magnitude, 2) the effects of ambient hydrostatic pressure and "live-load" forcing terms (i.e., terms that account for finite translations and rotations of the shell), 3) shell response at various locations, 4) the impact of flexural stiffness on mode participation, and 5) the accuracy of the doubly asymptotic approximation [8,10] for treatment of the fluid-structure interaction in dynamic elastic instability analysis. Conclusions drawn from the examination of these histories are listed in Section IV.

The present report may be regarded as contributing to the second stage of a three-stage study of the transient excitation of submerged, infinite cylindrical shells. The first stage, exemplified by References [7] and [11], deals with linear-elastic shell response. The second stage, exemplified by this report, deals with nonlinear-elastic shell response. The last stage, exemplified by Reference [12], deals with nonlinear-inealstic shell response. A corresponding study for spherical shells would be most useful, the first stage of which is exemplified by References [13] and [10].

SECTION 2

GOVERNING EQUATIONS

Consider the two-dimensional, plane-strain motions of the submerged, infinite, circular cylindrical shell shown in Figure 1. The shell is excited by a transient acoustic wave that first contacts the shell at $\theta = \pi$: The shell is thin and remains elastic at all times; geometric nonlinearity is considered, however, which introduces the possibility of dynamic instability.

2.1 ENERGY EXPRESSIONS

Kinetic and strain energy expressions for the cylindrical shell of Figure 1 are:

$$T = \frac{1}{2} \rho_o h \int_o^{2\pi} (\dot{v}^2 + \dot{w}^2)\, a d\theta$$

$$U = \frac{1}{2} \int_o^{2\pi} \int_{-h/2}^{h/2} \sigma_\theta \, \epsilon_\theta \, dz \, a d\theta \tag{1}$$

where $\dot{v} = \partial v/\partial t$, etc., σ_θ is the circumferential stress, ϵ_θ is the circumferential strain and z is the thickness coordinate. Stress-strain and strain-displacement relations for the shell are [14]

$$\sigma_\theta = \frac{E}{1-\nu^2} \epsilon_\theta$$

$$\epsilon_\theta = \frac{1}{a} \left(\frac{\partial v}{\partial \theta} + w\right) + \frac{1}{2a^2} \left(\frac{\partial w}{\partial \theta} - v\right)^2 - \frac{z}{a^2} \left(\frac{\partial^2 w}{\partial \theta^2} - \frac{\partial v}{\partial \theta}\right) \tag{2}$$

where only first-order geometric nonlinearities are considered. The introduction of (2) into (1) then yields

$$U = \frac{1}{2} \frac{Eh}{(1-\nu^2)a} \int_o^{2\pi} \left\{ \left[\frac{\partial v}{\partial \theta} + w + \frac{1}{2a} \left(\frac{\partial w}{\partial \theta} - v \right)^2 \right]^2 + \frac{h^2}{12a^2} \left(\frac{\partial^2 w}{\partial \theta^2} - \frac{\partial v}{\partial \theta} \right)^2 \right\} d\theta \tag{3}$$

An expression for the work potential appropriate to a pressure field acting on the surface of a smooth shell has been provided by Cohen [15]. For the present problem, that expression reduces to

$$\Pi = \int_0^{2\pi} \left[p\left(a + \frac{\partial v}{\partial \theta} + w\right) w + \frac{1}{2}\left(a\frac{\partial p}{\partial r} - p\right) w^2 + \frac{1}{2} p v^2 + v w \frac{\partial p}{\partial \theta} \right]_{r=a} d\theta \tag{4}$$

where $p = p(r, \theta, t)$ denotes the total pressure field. Although Cohen lists continuity of the pressure field as a requirement for the existence of the work potential, it is easily shown that a more lenient requirement is satisfactory, viz., that the pressure field contain a finite number of integrable discontinuities.

Now the displacement and pressure fields may be expanded in Fourier series as follows:

$$\begin{aligned} v(\theta, t) &\approx \sum_{n=1}^{\infty} v_n(t) \sin n\theta \\ w(\theta, t) &\approx \sum_{n=0}^{\infty} w_n(t) \cos n\theta \\ p(r, \theta, t) &\approx \sum_{n=0}^{\infty} p_n(r, t) \cos n\theta \end{aligned} \tag{5}$$

Also, the $n \neq 0$ Fourier coefficients for v and w may be transformed into extensional and flexural coefficients as follows [9]:

$$\begin{aligned} v_n &= n\, e_n - \frac{1}{n} f_n \\ w_n &= e_n + f_n \end{aligned} \tag{6}$$

The incorporation of (5) and (6) into (1), (3) and (4) then yields

$$\frac{T}{\pi\rho_o a h} = \dot{w}_o^2 + \frac{1}{2}\sum_{n=1}^{\infty}\left[(n^2+1)\,\dot{e}_n^2 + \left(\frac{n^2+1}{n^2}\right)\dot{f}_n^2\right]$$

$$\frac{U}{\pi Eh/(1-\nu^2)a} = w_o^2 + \frac{1}{2}\sum_{n=1}^{\infty}\left[(n^2+1)^2 e_n^2 + \frac{h^2}{12a^2}n^2\,(2n\,e_n + \frac{n^2-1}{n}f_n)^2\right]$$

$$+ \frac{1}{2}\frac{w_o}{a}\sum_{n=1}^{\infty} g_n^2 + \frac{1}{4a}\sum_{\ell=1}^{\infty}\sum_{m=1}^{\infty}\sum_{n=1}^{\infty}(\ell^2+1)\,e_\ell g_m g_n\,[\delta_{(m+\ell)n} + \delta_{(m-\ell)n}]$$

$$+ \frac{1}{32a^2}\sum_{k=1}^{\infty}\sum_{\ell=1}^{\infty}\sum_{m=1}^{\infty}\sum_{n=1}^{\infty} g_k g_\ell g_m g_n\,[\delta_{(k-\ell)o}\,\delta_{(m-n)o} + \delta_{(k-\ell)(m+n)}$$

$$- \delta_{(k+\ell)(m-n)} - \delta_{(k-\ell)(m+n)} + \delta_{(k+\ell)(m+n)}]$$

$$\frac{\Pi}{\pi a} = 2p_o^a w_o + \sum_{n=1}^{\infty} p_n^a\,(e_n + f_n) + \frac{1}{2}\frac{\partial p_o^a}{\partial r}\sum_{n=1}^{\infty}(e_n + f_n)^2$$

$$+ \frac{p_o^a}{2a}\sum_{n=1}^{\infty}\left[(3n^2+1)\,e_n^2 + 2(n^2-1)\,e_n f_n - \left(\frac{n^2-1}{n^2}\right)f_n^2\right]$$

$$+ \left(\frac{p_o^a}{a} + \frac{\partial p_o^a}{\partial r}\right)w_o^2 + \frac{w_o}{a}\sum_{n=1}^{\infty}\left(p_n^a + a\,\frac{\partial p_n^a}{\partial r}\right)(e_n + f_n)$$

$$+\frac{1}{2a}\sum_{n=1}^{\infty}\sum_{m=1}^{\infty}\{(p^a_{m-n}+p^a_{m+n})[(m+\tfrac{1}{2})\,e_m-\tfrac{1}{2}f_m]$$

$$+(\tfrac{a}{2})(\frac{\partial}{\partial r}p^a_{m-n}+\frac{\partial}{\partial r}p^a_{m+n})(e_m+f_m)\}(e_n+f_n)$$

$$+\frac{1}{2a}\sum_{n=1}^{\infty}\sum_{m=1}^{\infty}\{\tfrac{1}{2}(p^a_{m-n}-p^a_{m+n})(m\,e_m-\tfrac{1}{m}f_m)(n\,e_n-\tfrac{1}{n}f_n)$$

$$-[(m-n)\,p^a_{m-n}+(m+n)\,p^a_{m+n}](m\,e_m-\tfrac{1}{m}f_m)(e_n+f_n)] \qquad (7)$$

where $p^a_n = p_n(a,t)$, $\partial p^a_n/\partial r = [\partial p_n(r,t)/\partial r]_{r=a}$, $g_n = 2ne_n + [(n^2-1)/n]\,f_n$, $e_{m-n} = p_{m-n} = 0$ for $m \le n$, and the δ_{ij} are Kronecker deltas. Equations 7 constitute the basic energy expressions required for the present study.

2.2 ELIMINATION OF HIGH-ORDER TERMS

It is now appropriate to eliminate from (7) those terms of order higher than that necessary for a consistent formulation. For this purpose, the $n = 0$ pressure harmonic is taken to be of the order of the critical buckling pressure for the shell, which is [16]

$$P_C = \frac{Eh^3}{4(1-\nu^2)a^3} \qquad (8)$$

Hence $p^a_o \sim E(h/a)^3$, so that the two singly underlined terms in (7), which govern linear, static, axisymmetric response, yield $w_o/a \sim (h/a)^2$. Next, flexural displacements are taken as $f_n/a \sim h/a$, so that the doubly underlined terms, which govern linear, static, flexural response, yield $p^a_n \sim E(h/a)^4$. Finally, the triply underlined terms, which govern linear, static, nonaxisymmetric-extensional response, yield $e_n/a \sim (h/a)^3$. The use of these order-or-magnitude relations in (7), followed by the elimination of terms of order $(h/a)^6$ and higher, yields the simplified energy expressions

$$\frac{T}{\pi\rho_o ah} = \dot{w}_o^2 + \frac{1}{2}\sum_{n=1}^{\infty}(1+\frac{1}{n^2})\,\dot{f}_n^2$$

$$\frac{U}{\pi Eh/(1-\nu^2)a} = w_o^2 + \frac{1}{2}\sum_{n=1}^{\infty}\left[\frac{(\gamma h)^2}{12a^2}n^2 + \frac{w_o}{a}\right]\alpha_n^2 f_n^2 + \frac{1}{32a^2}\sum_{k=1}^{\infty}\sum_{\ell=1}^{\infty}\sum_{m=1}^{\infty}\sum_{n=1}^{\infty}\Delta_{k\ell mn}\,f_k f_\ell f_m f_n$$

$$\frac{\Pi}{\pi a} = 2p_o^a w_o + \sum_{n=1}^{\infty} p_n^a f_n - \frac{p_o^a}{2a}\sum_{n=1}^{\infty}\frac{\alpha_n}{n} f_n^2 + \frac{1}{2}\frac{\partial p_o^a}{\partial r}\sum_{n=1}^{\infty} f_n^2 \tag{9}$$

where $\alpha_n = (n^2-1)/n$ and $\Delta_{k\ell mn} = \alpha_k\alpha_\ell\alpha_m\alpha_n\,[\delta_{(k-\ell)o}\,\delta_{(m-n)o} + \delta_{(k-\ell)(m-n)} - \delta_{(k-\ell)(m+n)} + \delta_{(k+\ell)(m+n)}]$. Note that, because $\alpha_1 = 0$, the lower limits of six of the summations in (9) may be changed from 1 to 2.

A few remarks about (9) are in order. First, nonaxisymmetric-extensional response fails to appear as a significant energy contributor. Second, in the reduction of (7) to (9), it has been assumed that $a|\partial p_n^a/\partial r| \sim |p_n^a|$ for all n. Third, the last of (9) contains no nonlinear terms involving p_n; this implies that the last term in the integrand of (4) is unimportant. Fourth, a nondimensional parameter γ has been introduced into the flexural strain-energy term to permit consideration of a sandwich shell consisting of two concentric shells of thickness h/2 separated by a uniform core of negligible mass and in-plane stiffness. Such a shell serves as a convenient plane-strain model for a stiffened shell [7, 17]. With D as the sandwich shell's flexural stiffness, $\gamma^2 = 12(1-\nu^2)D/Eh^3$. Finally, the simplified expression for the shell's strain energy is positive-definite; this is readily seen by observing that, with $w(\theta,t) = w_o(t) + f(\theta,t)$, it constitutes a Fourier-series decomposition of the expression [cf. (3)]

$$U = \frac{1}{2}\frac{Eh}{(1-\nu^2)a}\int_o^{2\pi}\left\{\left[w_o + \frac{1}{2a}(f' + f^*)^2\right]^2 + \frac{(\gamma h)^2}{12a^2}(f'' + f)^2\right\} d\theta \tag{10}$$

where a prime denotes a θ-derivative and the asterisk a θ-integral. This corresponds to the use of Rayleigh's inextensibility assumption, i.e., $w = -\partial v/\partial\theta$ for nonaxisymmetric shell response [18].

It is interesting to examine results produced by (9) in certain special circumstances. First, consider the nonaxisymmetric, linear, free vibrations of a hydrostatically pressurized shell. In this case, $p_o(r,t) = P_H$, $p_n(r,t) = 0$ for $n \neq 0$, and the flexural displacements are infinitesimal. The application of Lagrange's equation [19]

$$\frac{d}{dt}\left(\frac{\partial L}{\partial \dot{q}}\right) - \frac{\partial L}{\partial q} = 0 \tag{11}$$

where $L = T - U - \Pi$, then yields, for $q = w_o$,

$$w_o = -\frac{(1-\nu^2)a^2}{Eh} P_H \tag{12}$$

For $q = f_n$, the application of Lagrange's equation yields

$$\rho_o \left(1 + \frac{1}{n^2}\right) \ddot{f}_n + \frac{E}{(1-\nu^2)a^2} \left\{ \left[\frac{(\gamma h)^2}{12a^2} n^2 + \frac{w_o}{a} \right] \alpha_n^2 - (1-\nu^2) \frac{P_H a}{Eh} \left(\frac{\alpha_n}{n} \right) \right\} f_n = 0 \qquad (13)$$

The introduction of (12) into (13), followed by the assumption of sinusoidal free vibration, yields the modal natural frequency equation

$$\omega_{fn}^2 = \left(\frac{c_o}{a}\right)^2 \frac{(\gamma h)^2}{12a^2} \left(\frac{n^2}{n^2+1}\right) (n^2-1)^2 \, (1-P_H/P_{Cn}) \qquad (14)$$

where $c_o^2 = E/\rho_o(1-\nu^2)$ is the plate velocity for the shell material and $P_{Cn} = \rho_o c_o^2 (h/a) \cdot (n^2-1) (\gamma h)^2/12a^2$ is the critical pressure for the nth flexural mode; note that $P_{C2} = P_C$ [cf. (8)]. Equation (14) clearly corresponds to the flexural frequency equation for a pressurized ring [20].

Next, consider the response of an unpressurized shell to nearly uniform radial impulse-excitation. The application of Lagrange's equation, (11), to the simplified energy expressions, (9), yields for axisymmetric extensional and nonaxisymmetric flexural response

$$(a/c_o)^2 \ddot{w}_o + w_o + \frac{1}{4a} \sum_{n=2}^{\infty} \alpha_n^2 f_n^2 = 0$$

$$(a/c_o)^2 \frac{n^2+1}{n^2} \ddot{f}_n + \left[\frac{(\gamma h)^2}{12a^2} n^2 + \frac{w_o}{a} \right] \alpha_n^2 f_n + \frac{1}{32a^2} \sum_{k=2}^{\infty} \sum_{\ell=2}^{\infty} \sum_{m=2}^{\infty} \Delta_{k\ell m}^{(n)} f_k f_\ell f_m = 0 \qquad (15)$$

where $\Delta_{k\ell m}^{(n)} = \Delta_{k\ell mn} + \Delta_{k\ell nm} + \Delta_{kn\ell m} + \Delta_{nk\ell m}$ and the discussion following (9) has been utilized.

These equations are similar to equations presented in [21-23], which treat this particular problem in considerable detail. Equations (15) are superior, in fact, to the corresponding equations in those references because only (15) exhibit <u>all</u> of the following characteristics: 1) n=1 rigid-body motion is decoupled from n=0 breathing motion,

2) linear-vibration frequencies for the flexural modes are given by the first of (14) with P_H=0, and 3) the associated strain energy expression is positive-definite.

From this brief examination of two special cases, it is concluded that (9) are suitable for the present analysis. This suitability derives from the consistent elimination of high-order terms from appropriate energy expressions.

2.3 FLUID-STRUCTURE INTERACTION

A rigorous formulation of the fluid-structure interaction, which must be considered in conjunction with (9), may be constructed as follows [7-9]. First, fluid pressure and radial fluid-particle velocity are expressed as derivatives of a fluid velocity potential as

$$p = -\rho \dot{\varphi}$$

$$u = \partial\varphi/\partial r \tag{16}$$

Second, the total acoustic field is treated as the superposition of an acoustic field for the (known) incident wave and an acoustic field for the (unknown) scattered wave, i.e.,

$$\varphi(r,\theta,t) = \varphi_I(r,\theta,t) + \varphi_S(r,\theta,t) \tag{17}$$

Third, compatibility of radial fluid-particle velocity and radial shell velocity is enforced at the wet surface of the shell as

$$u(a,\theta,t) = \dot{w}(\theta,t) \tag{18}$$

Finally, the wave equation and radiation condition for each circumferential harmonic of the scattered wave [see (5)] are replaced by the equivalent residual-potential relation

$$\frac{\partial\varphi_{Sn}}{\partial r} + \frac{1}{c}\dot{\varphi}_{Sn} + \frac{1}{2r}\varphi_{Sn} = \frac{1}{r}\varphi_{Rn} \tag{19}$$

in which the residual potential φ_{Rn} is given by the convolution relation

$$\varphi_{Rn}(r,t) = -\int_0^t r_n(r,t')\,\varphi_{Sn}(r,t-t')\,dt \tag{20}$$

where the r_n are characteristic functions that resemble step-exponential functions [7].

Equations 16-19 may now be utilized to produce, for each circumferential harmonic, the fluid-structure interaction relations

$$p_n^a = -\rho\,(\dot{\varphi}_{In}^a + \dot{\varphi}_{Sn}^a)$$

$$\frac{\partial p_n^a}{\partial r} = -\rho\,\ddot{w}_n$$

$$\dot{w}_n + \frac{1}{c}\dot{\varphi}_{Sn}^a + \frac{1}{2a}\varphi_{Sn}^a = u_{In}^a + \frac{1}{a}\varphi_{Rn}^a \tag{21}$$

where $\varphi_{Rn}^a = \varphi_{Rn}(a,t)$ is obtained from (20). These equations constitute the optimum form of the information required for a rigorous treatment of the fluid-structure interaction.

2.4 MODAL RESPONSE EQUATIONS

Convenient nondimensional equations may be obtained through introduction of the following convention:

$$\hat{p} = p^a/\rho c^2, \quad \hat{w} = w/a, \quad \hat{t} = ct/a \tag{22}$$

Application of this convention to (9) yields

$$\frac{T}{\pi\rho a^2 c^2} = \left(\frac{\rho_o h}{\rho a}\right)\left\{\dot{\hat{w}}_o^2 + \frac{1}{2}\sum_{n=1}^{\infty}\left(1+\frac{1}{n^2}\right)\dot{\hat{f}}_n^2\right\}$$

$$\frac{U}{\pi\rho a^2 c^2} = \left(\frac{\rho_o h}{\rho a}\right)\left(\frac{c_o}{c}\right)^2 \left\{ \hat{w}_o^2 + \frac{1}{2} \sum_{n=2}^{\infty} \left[\frac{(\gamma h)^2}{12a^2} n^2 + \hat{w}_o \right] \alpha_n^2 \hat{f}_n^2 + \frac{1}{32} \sum_{k=2}^{\infty}\sum_{\ell=2}^{\infty}\sum_{m=2}^{\infty}\sum_{n=2}^{\infty} \Delta_{k\ell mn} \hat{f}_k \hat{f}_\ell \hat{f}_m \hat{f}_n \right\}$$

$$\frac{\Pi}{\pi\rho a^2 c^2} = 2\hat{p}_o \hat{w}_o + \sum_{n=1}^{\infty} \hat{p}_n \hat{f}_n - \frac{1}{2} \hat{p}_o \sum_{n=2}^{\infty} \frac{\alpha_n}{n} \hat{f}_n^2 + \frac{1}{2} \hat{p}_o' \sum_{n=1}^{\infty} \hat{f}_n^2 \qquad (23)$$

where $\mathring{w}_o = d\hat{w}_o/d\hat{t}$, $\mathring{f}_n = d\hat{f}_n/d\hat{t}$, $\hat{p}_o' = [\partial \hat{p}_o/\partial \hat{r}]_{\hat{r}=1}$, and the discussion following (9) has been utilized. In like fashion, nondimensionalization of (21) and (20) yields

$$\hat{p}_n = -\left(\mathring{\varphi}_{In} + \mathring{\varphi}_{Sn}\right)$$

$$\hat{p}_n' = -\ddot{w}_n$$

$$\mathring{w}_n + \mathring{\varphi}_{Sn} + \frac{1}{2}\hat{\varphi}_{Sn} = \hat{u}_{In} + \hat{\varphi}_{Rn}$$

$$\hat{\varphi}_{Rn} = -\hat{r}_n * \hat{\varphi}_{Sn} \qquad (24)$$

where the asterisk denotes temporal convolution. Note that all nondimensional acoustic-field quantities in (23) and (24) pertain to the wet surface of the shell.

The application of Lagrange's equation, (11), to (23), followed by the appropriate utilization of (24) and the second of (6) with e_n neglected, yields the nondimensional modal response equations for the submerged shell

$$\mu \ddot{w}_o + \mu\beta w_o + \frac{1}{4}\mu\beta \sum_{n=2}^{\infty} \left(\frac{n^2-1}{n}\right)^2 f_n^2 - \mathring{\varphi}_{So} = \mathring{\varphi}_{Io}$$

$$\mu \frac{n^2+1}{n^2} \ddot{f}_n + \left\{ \mu\beta \left[\xi(n^2-1)^2 + \left(\frac{n^2-1}{n}\right)^2 w_o \right] + \frac{n^2-1}{n^2} \left(\mathring{\varphi}_{IO} + \mathring{\varphi}_{SO}\right) - \ddot{w}_o \right\} f_n$$

$$+ \frac{\mu\beta}{32} \sum_{k=2}^{\infty}\sum_{\ell=2}^{\infty}\sum_{m=2}^{\infty} \Delta_{k\ell m}^{(n)} f_k f_\ell f_m - \mathring{\varphi}_{Sn} = \mathring{\varphi}_{In}$$

$$\ddot{w}_o + \ddot{\varphi}_{So} + \frac{1}{2}\varphi_{So} = u_{Io} + \varphi_{Ro}$$

$$\ddot{f}_n + \ddot{\varphi}_{Sn} + \frac{1}{2}\varphi_{Sn} = u_{In} + \varphi_{Rn}$$

$$\varphi_{Rn} = -r_n * \varphi_{Sn} \tag{25}$$

where all circumflexes have been dropped, and where $\mu = \rho_o h/\rho a$, $\beta = (c_o/c)^2$ and $\xi = (\gamma h)^2/12a^2$. The nondimensional critical buckling pressure for the shell is, from (8), $P_C = 3\,\mu\,\beta\,\xi$.

Equations (25) constitute the modal response equations needed for a rigorous analysis of the nonlinear dynamic response of a submerged, infinite, elastic, circular, cylindrical sandwich shell excited by a transverse, transient acoustic wave. They lend themselves to step-by-step numerical integration in time, producing modal response histories that, through (6) with e_n neglected and through (5), yield corresponding shell response histories. From (2), (5), and (6) with e_n neglected, extensional and flexural strain response histories may be obtained as

$$\varepsilon_\theta^e = w_o + \frac{1}{2}\left(\sum_{n=1}^{\infty}\frac{n^2-1}{n} f_n \sin n\theta\right)^2$$

$$\varepsilon_\theta^f = z\sum_{n=1}^{\infty}(n^2-1)\, f_n \cos n\theta \tag{26}$$

where z is nondimensional [see (22)]. For the sandwich shell described after (9), the distance from the neutral axis to the outer shell fiber is given by

$$|z|_{max} = \frac{h}{4}\left[1 + \sqrt{1 + \frac{4}{3}(\gamma^2-1)}\right] \tag{27}$$

SECTION 3

NUMERICAL RESULTS

The numerical results presented in this section have been generated by the application of fourth-order Runge-Kutta numerical integration to the first four of (25) and the use of trapezoidal integration for the last of (25). A variable incrementing procedure with $0.002 \leq \Delta t \leq 0.2$, has been used. Results have been obtained for two steel shells submerged in sea water, all characterized by $\rho_o/\rho = 7.72$, $c_o/c = 3.53$ and $a/h = 100$. The two shells differ in terms of their γ-values, which are 5 and 10; these values correspond to moderate and heavy stiffening of a uniform homogeneous shell. The shells are excited by plane acoustic waves of rectangular and exponential pressure profile that make initial contact at time $t = 0$ along the line $\theta = \pi$. The generalized excitation functions for these waves are given by

$$\overset{\circ}{\varphi}_{In}(t) = (-1)^{n+1} \frac{\varepsilon_n}{\pi} P_I \int_0^{\pi} g(t - 1 + \cos\zeta) \cos n\zeta \, d\zeta$$

$$u_{In}(t) = (-1)^{n+1} \frac{\varepsilon_n}{\pi} P_I \int_0^{\pi} g(t - 1 + \cos\zeta) \cos\zeta \cos n\zeta \, d\zeta \qquad (28)$$

where $\varepsilon_n = 1$ for $n = 0$ and $\varepsilon_n = 2$ for $n \geq 1$, and P_I is the maximum value of the incident-wave pressure profile. For the rectangular wave, $g(t) = H(t) - H(t-T)$, where $H(t)$ is the Heaviside step-function and T is the pulse duration; for the exponential wave, $g(t) = H(t)\, e^{-\lambda t}$, where λ is the decay constant. Note that all of the preceding quantities are nondimensional, having been normalized in accordance with (22).

3.1 MODAL RESPONSE

Figure 2 shows displacement response histories for the (n=0) breathing mode of the $\gamma = 10$ sandwich shell when excited by broad, rectangular, incident waves of duration $T = 10$. The pressure magnitudes of these waves vary from 1% to 300% of the critical buckling pressure for the shell [see (8), or the discussion following (25)]. Note that all responses are normalized to the magnitude of the incident wave, so that coalescence of response histories implies linearity of response. In this connection, it is seen that the response for $P_I = P_C$ and $P_I = 2P_C$ are virtually coincident with the (linear) response for $P_o = 0.01\, P_C$; nonlinear effects are discernible for $P_I = 3P_C$, but they are relatively unimportant.

Velocity response histories for the (n=1) translational mode are shown in Figure 3. Nonlinear effects are barely discernible. This implies that the last term in the last of (23) is of negligible importance because, without it, the n=1 mode is totally uncoupled from the other modes and is governed by purely linear equations [see (25) and the second of (24)].

The n=2 lobar mode is the one that exhibits significant nonlinear behavior, as shown by the displacement response histories of Figure 4. The response may be conveniently described as occurring in four phases: an "envelopment phase", which extends from t=0 to t=2, a "pressurization phase", which extends from t=2 to t=T, a "development phase", which extends from t=T to t=T+2, and a "free-vibration phase", which extends onward from t=T+2. During the envelopment phase, in which the incident wave front is passing over the shell, the response is essentially linear. The pressurization phase, in which the shell is essentially hydrostatically pressurized by the incident wave, is characterized by either oscillatory or exponential response, depending upon the magnitude of P_I. During the development phase, in which the back of the rectangular incident wave is passing over the shell, the response exhibits sudden, but modest reversal. Finally, the free-vibration phase is characterized by low-frequency sinusoidal motion. Clearly, the appearance of response overshoot during the free vibration phase depends upon exponential growth experienced during the pressurization phase, which, in turn, depends upon the magnitude of P_I.

Displacement response histories for the n=3 lobar mode are shown in Figure 5. The preceding description of n=2 response is applicable here also. Especially visible in the n=3 response histories is the virtually undamped nature of the sinusoidal motions during the free-vibration phase. This indicates that the surrounding fluid provides very small acoustic radiation damping for these motions, which is to be expected when the characteristic structural wavelength $2\pi a/n$ is much smaller than the acoustic wavelength c/f, where f is the frequency of oscillation [1]. The n=4 and n=5 lobar modes have been included in these $\gamma = 10$ shell calculations, but exhibit peak displacements substantially smaller than that of the n=3 mode. Hence response histories are not shown for these modes.

It is instructive to examine dynamic instability of the flexural modes during the pressurization phase. During this phase, n=0 displacement is approximately equal to the hydrostatic value

$$w_o(t) \approx - \frac{P_I}{\mu\beta} \tag{29}$$

Also, flexural response is relatively slow, so that $\dot{\varphi}_{Sn} << \varphi_{Sn}$ and, from the last of (25) and [7],

$$\varphi_{Rn} \approx -\varphi_{Sn}\int_{o}^{\infty} r_n(t')dt' = -(n-\tfrac{1}{2})\,\varphi_{Sn} \tag{30}$$

Hence the fourth of (25) yields, with $u_{In} = 0$ for $n \geq 2$, $2 \leq t \leq T$ [9],

$$\varphi_{Sn} \approx -\frac{1}{n}\,\mathring{f}_n \tag{31}$$

Equations (29) and (31), along with the approximations $\mathring{\varphi}_{So} \approx 0$, $\overset{\circ\circ}{w}_o \approx 0$ and neglect of the triple summation in the second of (25), yield for flexural response during the pressurization phase

$$(\mu\,\frac{n^2+1}{n^2} + \frac{1}{n})\,\overset{\circ\circ}{f}_n + (n^2-1)\,(P_{Cn} - P_I)\,f_n = 0 \tag{32}$$

where $P_{Cn} = (n^2-1)\mu\beta\xi$. This equation exhibits the effect of added fluid mass associated with low-frequency shell response; it also indicates that shell response is oscillatory for $P_I < P_{Cn}$ and exponential for $P_I > P_{Cn}$, as seen in Figures 4 and 5. It is worth noting that with the removal of P_I, (32) also governs flexural mode response during the free-vibration phase.

Modal response histories for excitation by incident step-exponential waves with decay constant $\lambda = 1$ are shown in Figures 6-9. The normalized responses are substantially smaller than their rectangular-wave-excitation counterparts in Figures 2-5 because of the reduction in pulse width. Otherwise, the behavior is similar, with significant nonlinear effects appearing only in the $n \geq 2$ harmonics.

3.2 AMBIENT HYDROSTATIC PRESSURE AND LIVE LOAD

It is interesting to examine the effects of ambient hydrostatic pressure on the shock response of the $\gamma = 10$ shell. The modifications in (25) required for such an examination merely involve the replacement of w_o by $w_o - P_H/\mu\beta$ and of $\mathring{\varphi}_{Io}$ by $\mathring{\varphi}_{Io} - P_H$, where P_H is the magnitude of the hydrostatic pressure. With these replacements, the first of (25) remains the same, except that it now pertains to breathing motions about a static equilibrium radius of $1 - P_H/\mu\beta$. The second of (25) changes only to the extent that the term $\xi(n^2-1)^2$ is now multiplied by $(1 - P_H/P_{Cn})$, where P_{Cn} is given after (32).

For static stability, P_H must be less than the smallest of the P_{Cn}, which is $P_{C2} = P_C = 3\mu\beta\xi$. Hence the reduction in static equilibrium radius cannot exceed 3ξ, which is very small. Thus the principal effect of ambient hydrostatic pressure is the reduction of flexural stiffness, which is a destabilizing influence.

It is also interesting to examine inaccuracies introduced into transient response computations by the neglect of the "live-load" terms in (4). These terms account for the

effects of finite translations and rotations of the shell on the work done by the normal pressure loading as referenced to the undeformed shell surface. All the terms in (4) except p•a•w are live-load terms; when processed through the Fourier-decomposition and term-elimination operations of Subsections 2.1 and 2.2, they appear in nondimensional form as the last two summation terms in the last of (23). Following the application of Lagrange's equation (11) and the introduction of the fluid-structure interaction equations (24), live-load effects manifest themselves as the terms $[(n^2-1)/n^2]\ (\mathring{\varphi}_{Io} + \mathring{\varphi}_{So})$ and $-\overset{\circ\circ}{w}_o$ in the second of (25).

Response computations designed to demonstrate the effects of ambient hydrostatic pressure and live load have been performed for the $\gamma = 10$ sandwich shell excited by both $T = 10$, $P_I = 2P_C$ rectangular and $\lambda = 1$, $P_I = 5P_C$ exponential incident waves. As would be expected, n=0 and n=1 response is unaffected by the introduction of ambient hydrostatic pressure or the omission of live-load terms in (25). In contrast, the response behavior of the n=2 flexural mode is substantially affected, as indicated in Figures 10 and 11. It is clear from these figures that ambient hydrostatic pressure and live load are both significant destabilizing influences for this mode*. The higher modes are much less influenced, however, as indicated by the n=3 response histories of Figures 12 and 13.

3.3 SHELL RESPONSE

Modal response histories for $0 \leq n \leq 5$ have been superposed in accordance with (5) and (26) to construct the shell response histories of Figures 14-19. Figures 14, 16 and 18 pertain to excitation by a $T = 10$, $P_I = 2P_C$ rectangular incident wave, while Figures 15, 17 and 19 pertain to excitation by a $\lambda = 1$, $P_I = 5P_C$ exponential incident wave.

Shown in Figures 14 and 15 are deformational displacement histories, which constitute displacement histories with rigid-body motion removed, i.e., $w_D(\theta,t) = w(\theta,t) - f_1(t)\cos\theta$. It is seen that the effects of ambient hydrostatic pressure and live load are significant for excitation by the rather broad rectangular pulse, but are relatively minor for excitation by the rather narrow exponential pulse.

Figures 16 and 17 show radial velocity histories at two points on the shell. The effects of the ambient hydrostatic pressure and live load are clearly negligible. Strain response histories are shown in Figures 18 and 19 at locations selected to emphasize flexural and nonlinear-extensional contributions to total strain. The coincidence of the w_o- and ε^e_θ-histories in the figures demonstrates that the nonlinear-extensional term in the first

* A development like that which produced (32), but which includes ambient hydrostatic pressure and excludes live-load terms, leads to a prediction of the coalescence, for $0 \lesssim t \lesssim 10$, of the response histories of Figure 10 with the circle and triangle designators.

of (26) is minuscule. This, along with the smallness of the flexural strain history, demonstrates that the strain response of the shell is dominated by the n=0 breathing mode. Hence, peak strain in the shell is accurately estimated as

$$|\varepsilon|_{max} \approx (P_I^{-1} |w_o|_{max}) \cdot NP_C \tag{33}$$

where $N = P_I/P_C$. For the shell of Figure 2, for example, $P_I^{-1}|w_o|_{max} = 1.125$ and $P_C = 3\mu\beta\xi = 2.405 \times 10^{-3}$; hence $|\varepsilon|_{max} \approx 0.27N\%$, as suggested by Figure 18.

3.4 FLEXURAL STIFFNESS EFFECTS

It is informative to compare the response behavior of a moderately stiffened ($\gamma = 5$) shell with that of the heavily stiffened ($\gamma = 10$) shell of Figures 2-19. As the flexural stiffness of a sandwich shell is proportional to γ^2 [see the discussion preceding (10)], the P_C-value for the moderately stiffened shell is only one-quarter of that for the heavily stiffened shell. Hence, in order to maintain proper calibration between the excitation levels for the two shells, P_I-values of 0.04 P_C, 4 P_C, 8 P_C, and 12 P_C are used for the moderately stiffened shell.

Figures 20-24 show modal response histories for the $\gamma = 5$ shell. A comparison of the first of these with Figure 2 indicates that nonlinear effects in n=0 response are more pronounced for the $\gamma = 5$ shell than they are for the $\gamma = 10$ shell; even so, they remain relatively unimportant. Figure 21, which pertains to n=1 response, is virtually a duplicate of Figure 3, in which nonlinear effects are barely discernible.

Figure 22, which pertains to n=2 response, displays significant nonlinear behavior, as does Figure 4 for the $\gamma = 10$ shell. For the same value of $P_I \geq P_C$, an n=2 response peak during the free-vibration phase for the $\gamma = 5$ shell considerably exceeds its counterpart for the $\gamma = 10$ shell. This is suggested by (32), which predicts exponential response growth for $P_I > P_{C2} = P_C$ during the pressurization phase. For example, for the $\gamma = 5$ shell with $P_I = 12\ P_C$, the stiffness coefficient multiplying f_2 is $-3{\cdot}11{\cdot}P_C = -99{\cdot}\mu\beta{\cdot}25h^2/12a^2$, which exceeds in magnitude its counterpart for the $\gamma = 10$ shell with $P_I = 3\ P_C$, which is $-3{\cdot}2{\cdot}P_C = -18{\cdot}\mu\beta{\cdot}100h^2/12a^2$. In contrast to the $P_I \geq P_C$ results of Figure 22, the peak free-vibration-phase response of the $\gamma = 5$ shell for $P_I = 0.04\ P_C$ is only one-half that of the $\gamma = 10$ shell for $P_I = 0.01\ P_C$. This may be explained as follows. An approximate expression for the linear, post-envelopment, n=2 response of a step-wave-excited shell is given in [24]. This expression, in turn, leads to the following expression for n=2, linear, free-vibration-phase response appropriate to excitation by a rectangular incident wave whose duration T is much smaller than the n=2 mode's natural period of oscillation during the free-vibration phase:

$$f_2(t) \approx \frac{4/5}{2\mu + 4/5} P_I \Omega_2 \sin\Omega_2 (t - \tfrac{1}{2}T) \qquad (34)$$

where $\Omega_2^2 = 36\mu\beta\xi/(5\mu+2)$. Hence, inasmuch as ξ for the $\gamma = 10$ shell is four times that for the $\gamma = 5$ shell, peak free-vibration response of the $\gamma = 10$ shell for $P_I << P_C$ is double that of the $\gamma = 5$ shell, all other parameters being equal.

It is clear from the preceding paragraph that the nonlinear response of a flexural mode to rectangular-wave excitation depends critically upon the "initial conditions" for the pressurization and free-vibration phases and the value of the pressurization-phase "stiffness" parameter in (32). With $P_I = NP_C$, (32) predicts exponential growth during the pressurization phase for those modes whose modal index satisfies the inequality $n < (3N+1)^{\frac{1}{2}}$. Hence a large value of N implies that many flexural modes may contribute significantly to shell response, while a small value of N implies that only the lowest flexural modes need be considered. This is illustrated in Figures 23 and 24, which show modal response histories for n=3 and 4. Although the n=3 response peaks for the $\gamma = 5$ shell are no larger than their counterparts for the $\gamma = 10$ shell shown in Figure 5, the n=4 mode of the $\gamma = 5$ shell responds strongly, especially for $P_I = 12\ P_C$. This is in contrast to n=4 response for the $\gamma = 10$ shell, which is so small that it is not even included in the discussion of Subsection 3.1.

The increased participation of the higher flexural modes in the response of the $\gamma = 5$ shell suggests that flexural strain might now play a much more important role than that portrayed in Figure 18 for the $\gamma = 10$ shell. This is not the case, however, as shown in Figure 25, because the increase in flexural mode response is essentially negated by the decrease in the distance between the outer fibers of the shell. There is a discernible nonlinear-extensional contribution to total strain, but it is hardly significant.

The preceding comparison of $\gamma = 5$ and $\gamma = 10$ shell response illustrates the dissimilarities between the response behavior of moderately stiffened and heavily stiffened shells to a given incident wave. The contrast between an unstiffened shell and a moderately stiffened shell is even greater. For example, $P_I = 8\ P_C$ for $\gamma = 5$ corresponds to $P_I = 200\ P_C$ for $\gamma = 1$. Thus, while (32) predicts exponential growth during the pressurization phase for the $n < 5$ flexural modes of the $\gamma = 5$ shell, it predicts such growth for the $n < 25$ flexural modes of the $\gamma = 1$ shell. Experimental observations of such short-structural-wavelength instability are reported in [25, 26].

3.5 DOUBLY ASYMPTOTIC APPROXIMATION

As mentioned in Section 1, an aspect of particular interest in the present study has been the accuracy of the doubly asymptotic approximation (DAA) [8, 10] for treatment of the fluid-structure interaction. In the present context, such treatment involves replacement

of the coefficient $\frac{1}{2}$ in the third and fourth of (25) by n, omission of φ_{Rn} in those equations, and omission of the last of (25) entirely. With these changes, modal response histories have been calculated for direct comparison with the exact histories of Figures 2-9 produced by the residual potential formulation (RPF).

Modal response histories pertaining to rectangular-wave excitation of the $\gamma = 10$ shell are shown in Figures 26-29. Two of the four histories in each figure pertain to the largest incident-wave magnitude considered in Figures 2-5, while the other two pertain to an incident-wave magnitude so small that linear shell response is assured. An examination of Figures 26-29 reveals that discrepancies between the DAA and RPF histories for $P_I = 3\ P_C$ are similar in nature and size to those between the DAA and RPF histories for $P_I = 0.01\ P_C$. This indicates, of course, that DAA accuracy for elastic dynamic instability calculations is fully comparable to that for linear-elastic response calculations. In particular, the tendency of the DAA to overestimate acoustic radiation damping for low-frequency free vibration does not artificially suppress unstable shell response during the pressurization phase.

A comparison of DAA and RPF response histories for exponential-wave excitation of the $\gamma = 10$ shell leads to the conclusions expressed in the previous paragraph. Hence exponential-wave counterparts to Figures 26-29 need not be shown. A thorough examination of the accuracy of the DAA for linear-elastic shell response is provided in [27].

SECTION 4

CONCLUSION

This study has dealt with the dynamic instability of an infinite, elastic, submerged, circular cylindrical shell excited by a transverse, transient acoustic wave. Circumferential Fourier decomposition of the field quantities appearing in appropriate energy functionals, followed by consistent elimination of high-order terms, has led to rather simple shell response equations with satisfactory attributes. The fluid-structure interaction has been treated rigorously in accordance with the residual potential formulation, which has been used successfully in a number of previous studies.

Numerical results have been presented in the form of 117 transient response histories pertaining to excitation by plane waves of rectangular and exponential pressure-profile. Examination of these results has led to the following conclusions:

1. Dynamic instability effects are significant only with respect to flexural shell response.
2. The dynamically unstable flexural response that occurs while the incident-wave profile passes over the shell profoundly affects subsequent free-vibration flexural response.
3. For peak total strains smaller than 1%, only the lowest flexural modes of a heavily stiffened shell experience dynamic instability; if the degree of stiffening is reduced, however, higher flexural modes exhibit such instability until, in the limit of an unstiffened shell, numerous flexural modes are involved. Hence, the response of an unstiffened shell to a given incident wave is significantly different than that of an appreciably stiffened shell to the same wave.
4. n=0 breathing motion dominates strain response, and quasi-linear (especially n=1 translational) motions dominate velocity response; nonlinear flexural motions are important only with regard to deformational displacement response, i.e., displacement response exclusive of rigid-body translation.
5. As a consequence of the preceding conclusions, live-load forcing terms and ambient hydrostatic pressure substantially affect deformational displacement response, but have minor impact on velocity and strain response.
6. The live-load terms in the surface-pressure work potential that involve pressure gradients may be neglected [see (4)].
7. The accuracy of the doubly asymptotic approximation for treatment of the fluid-structure interaction in dynamic elastic-instability calculations is fully comparable to that observed in linear-elastic response calculations.

SECTION 5

REFERENCES

1. Geers, T. L., "Transient Response Analysis of Submerged Structures", pp 59-84 of Finite Element Analysis of Transient Nonlinear Structural Behavior, T. Belytschko, J. R. Osias and P. V. Marcal, eds., AMD-Vol. 14, ASME, New York, 1975.

2. DiMaggio, F. L., "Effect of an Acoustic Medium on the Dynamic Buckling of Plates", J. Appl. Mech., Vol. 23, No. 2, June 1956, pp 201-206.

3. Deng, Z.-F. and Popelar, C. H., "Dynamic Stability of a Cylindrical Shell in an Acoustic Medium", J. Acoust. Soc. Am., Vol. 52, No. 5, Nov. 1972, pp 1430-1436.

4. Mnev, Y. N., and Pertsev, A. K., Hydroelasticity of Shells, FTD-MT-24-119-71, Foreign Technology Division, Wright-Patterson Air Force Base, OH, August 1971.

5. Grigoliuk, E. I., and Gorshkov, A. G., Nonstationary Hydroelasticity of Shells, Sudostroenie, Leningrad, 1974; translated by M. D. Friedman, LMSC-D567983, Lockheed Missiles and Space Company, Sunnyvale, CA, November 1977.

6. Longhitano. R., and Klosner, J. M., "Nonlinear Dynamics of Submerged Hemispherical Shells", AE/AM Rpt. No. 74-4, Polytechnic Institute of New York, New York, Feb. 1974.

7. Geers, T. L., "Excitation of an Elastic Cylindrical Shell by Transient Acoustic Wave", J. Appl. Mech., Vol. 36, No. 3, Sept. 1969, pp 459-469.

8. Geers, T. L., "Residual Potential and Approximate Methods for Three-Dimensional Fluid-Structure Interaction Problems", J. Acoust. Soc. Am., Vol. 49, No. 5, May 1971, pp 1505-1510.

9. Geers, T. L., "Scattering of a Transient Acoustic Wave by an Elastic Cylindrical Shell", J. Acoust. Soc. Am., Vol. 51, No. 5, May 1972, pp 1640-1651.

10. Geers, T. L., "Doubly Asymptotic Approximations for Transient Motions of Submerged Structures". J. Acoust. Soc. Am., Vol. 64, No. 5, Nov. 1978, pp 1500-1508.

11. Huang, H., "An Exact Analysis of the Transient Interaction of Acoustic Plane Waves with a Cylindrical Elastic Shell", J. Appl. Mech., Vol. 37, No. 4, Dec. 1970, pp 1091-1106.

12. Geers, T. L., and Yen, C. L., "Inelastic Response of an Infinite Cylindrical Shell to a Transient Acoustic Wave", LMSC-D676214, Lockheed Palo Alto Research Laboratory, Palo Alto, CA, March 1979.

13. Huang, H., "Transient Interaction of Plane Acoustic Waves with a Spherical Elastic Shell", J. Acoust. Soc. Am., Vol. 45, No. 3, March 1969, pp 661-670.

14. Sanders, J. L., "Nonlinear Theories for Thin Shells", Q. Appl. Math., Vol. 21, No. 1, April 1963, pp 21-36.

15. Cohen, G. A., "Conservativeness of a Normal Pressure Field Acting on a Shell", AIAA J., Vol. 4, No. 10, Oct. 1966, p 1886.

16. Brush, D. O., and Almroth, B. O., Buckling of Bars, Plates, and Shells, McGraw-Hill Book Co., New York, N.Y., 1975.

17. Forrestal, M. J., Response of an Elastic Cylindrical Shell to a Transverse Acoustic Pulse", J. App. Mech., Vol. 35, No. 3, Sept. 1968, pp 614-616.

18. Lord Rayleigh, Theory of Sound, 2nd Ed., Vol. 2, Dover Press, New York, N.Y., 1975.

19. Slater, J. C., and Frank, N. H., Mechanics, McGraw-Hill Book Co., New York, N.Y., 1947.

20. Liessa, "Vibration of Shells", NASA SP-288, National Aeronautics and Space Administration., Washington, D.C., 1973.

21. Goodier, J. N., and McIvor, I. K., "The Elastic Cylindrical Shell Under Nearly Uniform Radial Impulse", J. Appl. Mech., Vol. 31, No. 2, June 1964, pp 259-266.

22. Lindberg, H. E., "Stress Amplification in a Ring Caused by Dynamic Instability", J. Appl. Mech., Vol. 41, No. 2, June 1974, pp 392-400.

23. Hubka, W. F., "Dynamic Buckling of the Elastic Cylindrical Shell Subjected to Impulsive Loading", J. Appl. Mech., Vol. 41, No. 2, June 1974, pp 401-411.

24. Geers, T. L., "Response of an Elastic Cylindrical Shell to a Transverse Acoustic Shock Wave in a Light Fluid Medium", J. Acoust. Soc. Am., Vol. 48, No. 3, Sept. 1970, pp 692-701.

25. Anik'ev, I. I., Vorotnikova, M. I., and Kononenko, V. O., "Some Experimental Results on the Effect of a Lateral Shock Wave in Water on Cylindrical Shells", Prikladnaia Mekhanika, Vol. 7, No. 9, 1971, pp 106-109.

26. Anik'ev, I. I., and Vorotnikova, M. I., "An Experimental Method for Investigating Nonsteady-State Deformation of Shells Acted on by a Shock Wave", Izv. ANSS R, Mekhanika Tverdogo Tela, Vol. 10, No. 6, 1975, pp 141-145.

27. Geers, T. L., "Shock Response Analysis of Submerged Structures", Shock and Vibration Bulletin, Vol. 44, Supp. 3, Aug. 1974, pp 17-32.

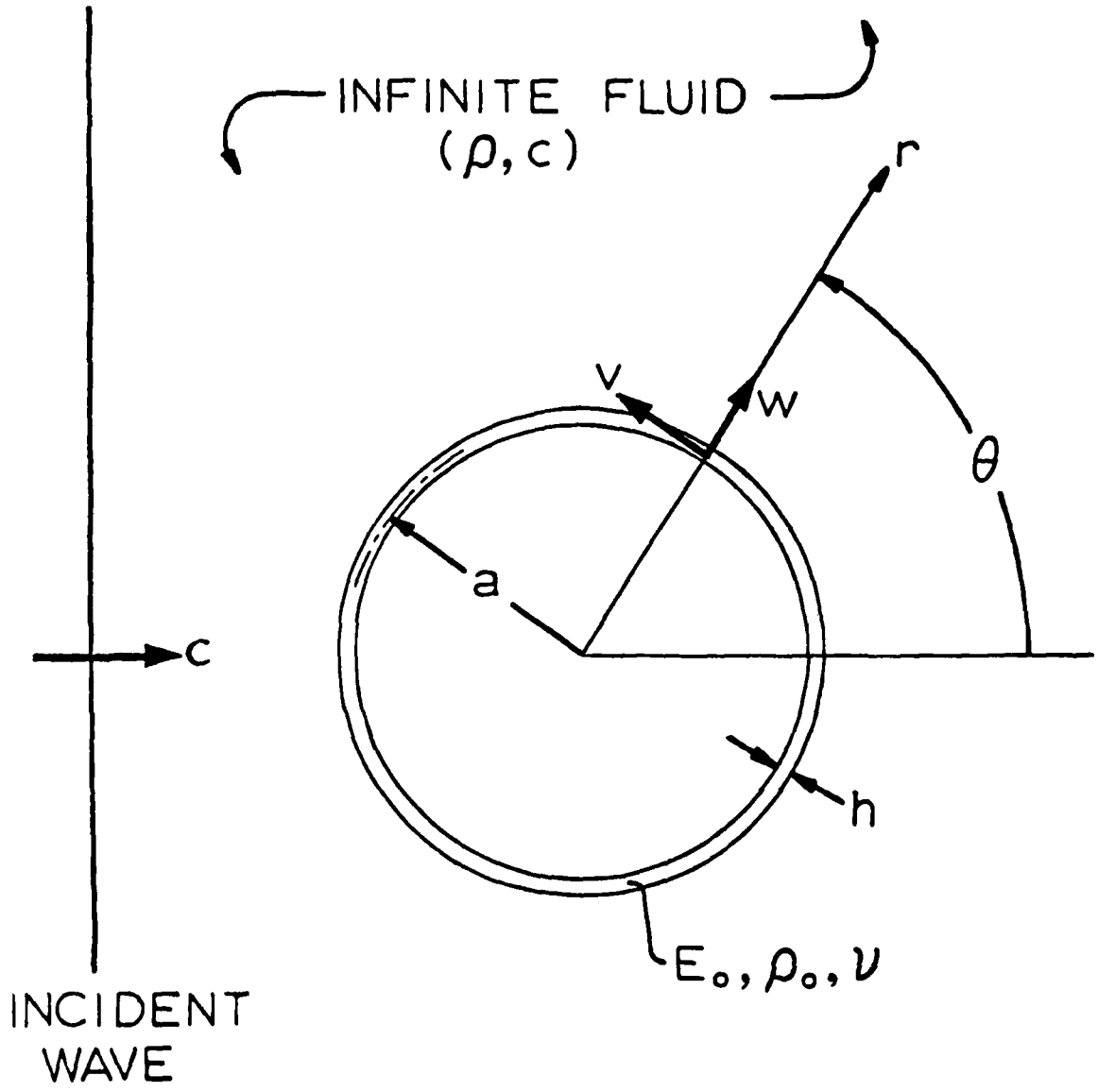

FIGURE 1. Infinite, Elastic, Circular Cylindrical Shell Submerged in an Infinite Acoustic Medium.

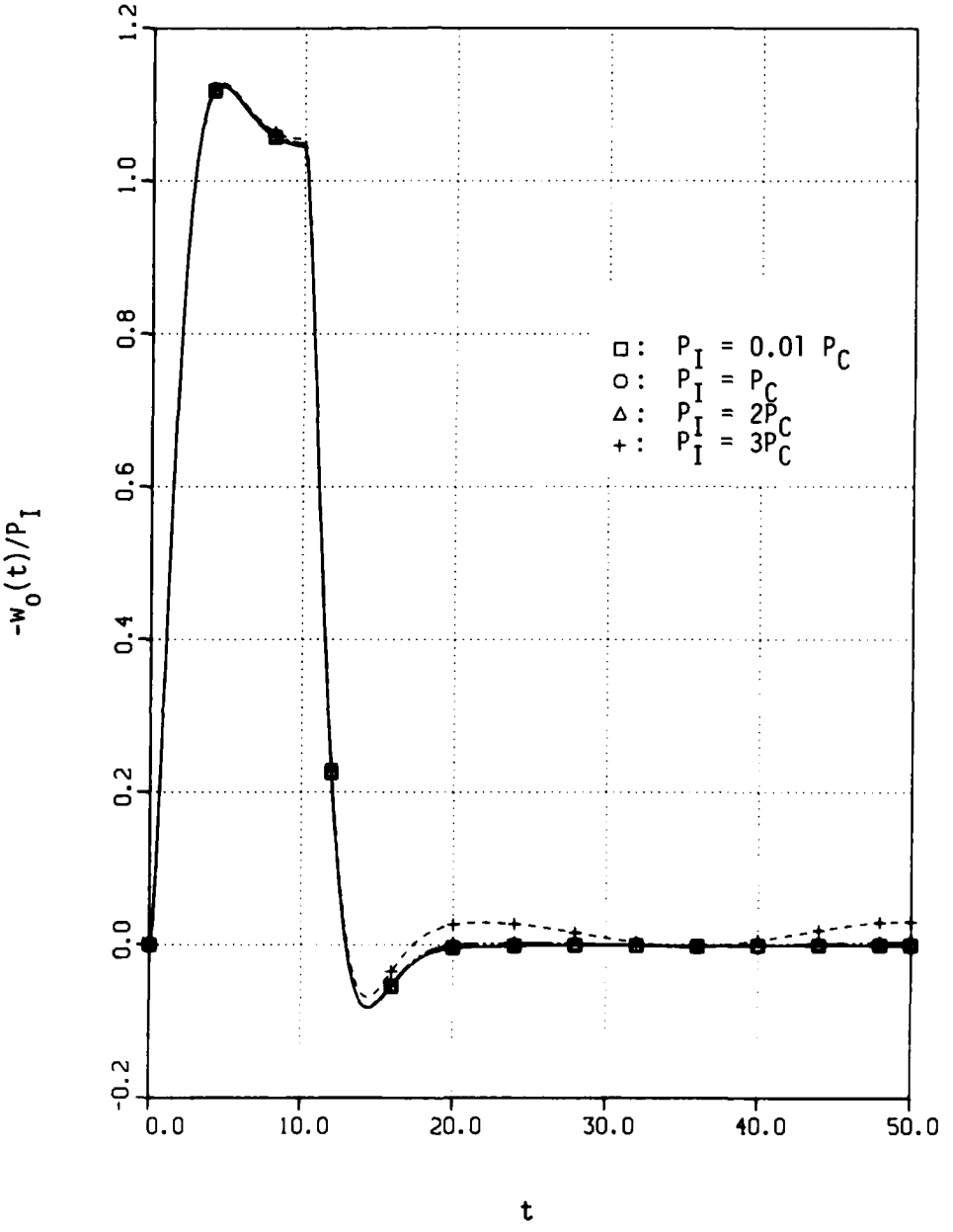

FIGURE 2. n=0 Displacement Response of the $\gamma = 10$ Shell to Rectangular Incident Waves with $T = 10$.

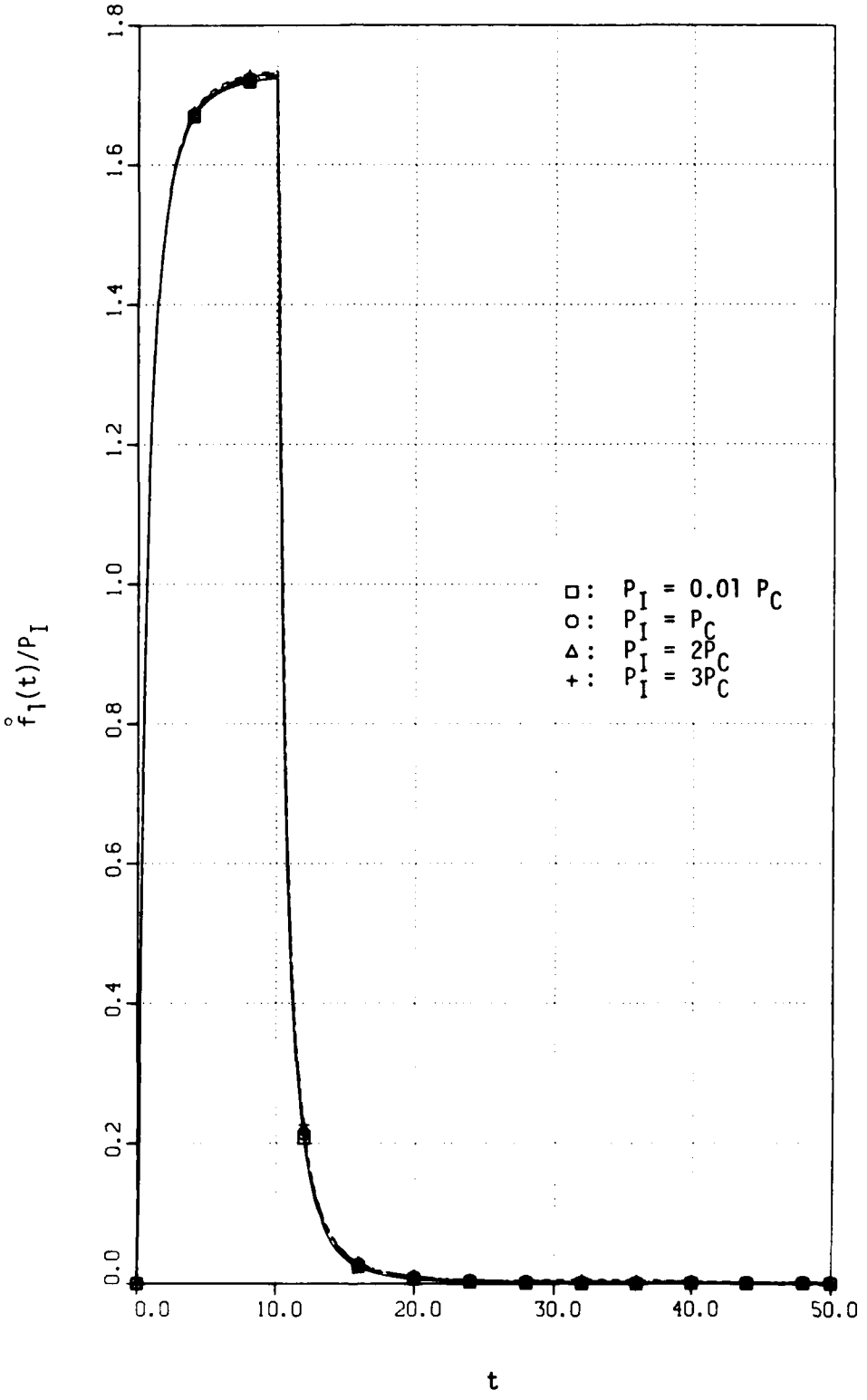

FIGURE 3. n=1 Velocity Response of the $\gamma = 10$ Shell to Rectangular Incident Waves with T = 10.

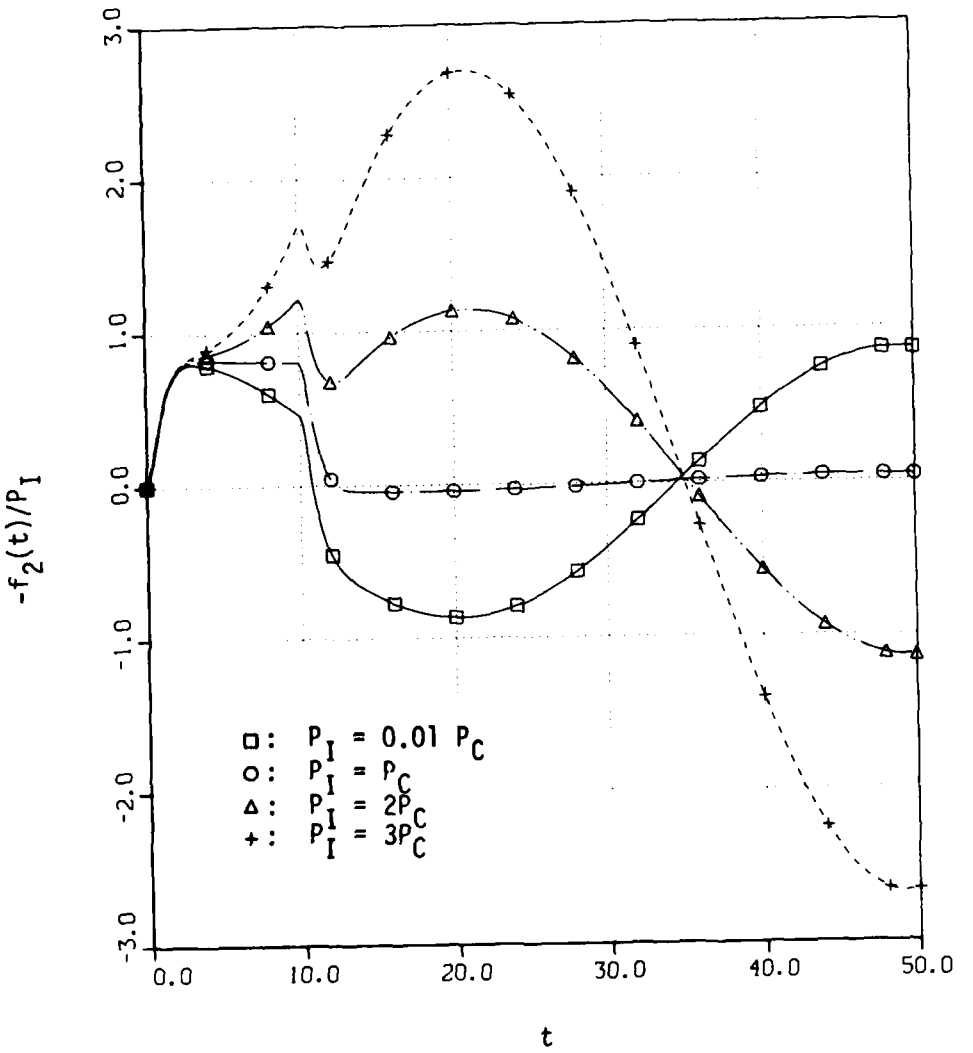

FIGURE 4. n=2 Displacement Response of the $\gamma = 10$ Shell to Rectangular Incident Waves with T = 10.

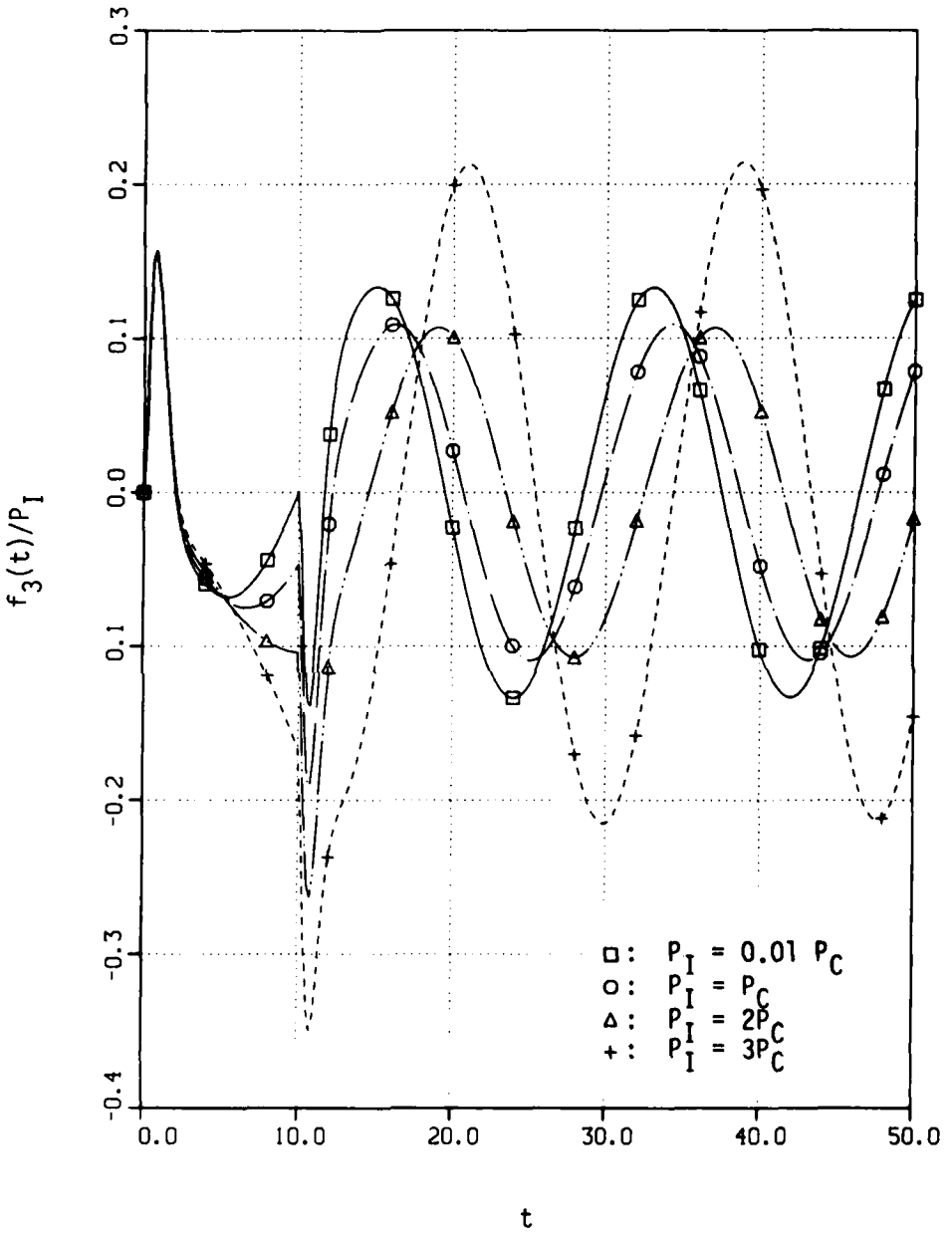

FIGURE 5. n=3 Displacement Response of the $\gamma = 10$ Shell to Rectangular Incident Waves with $T = 10$.

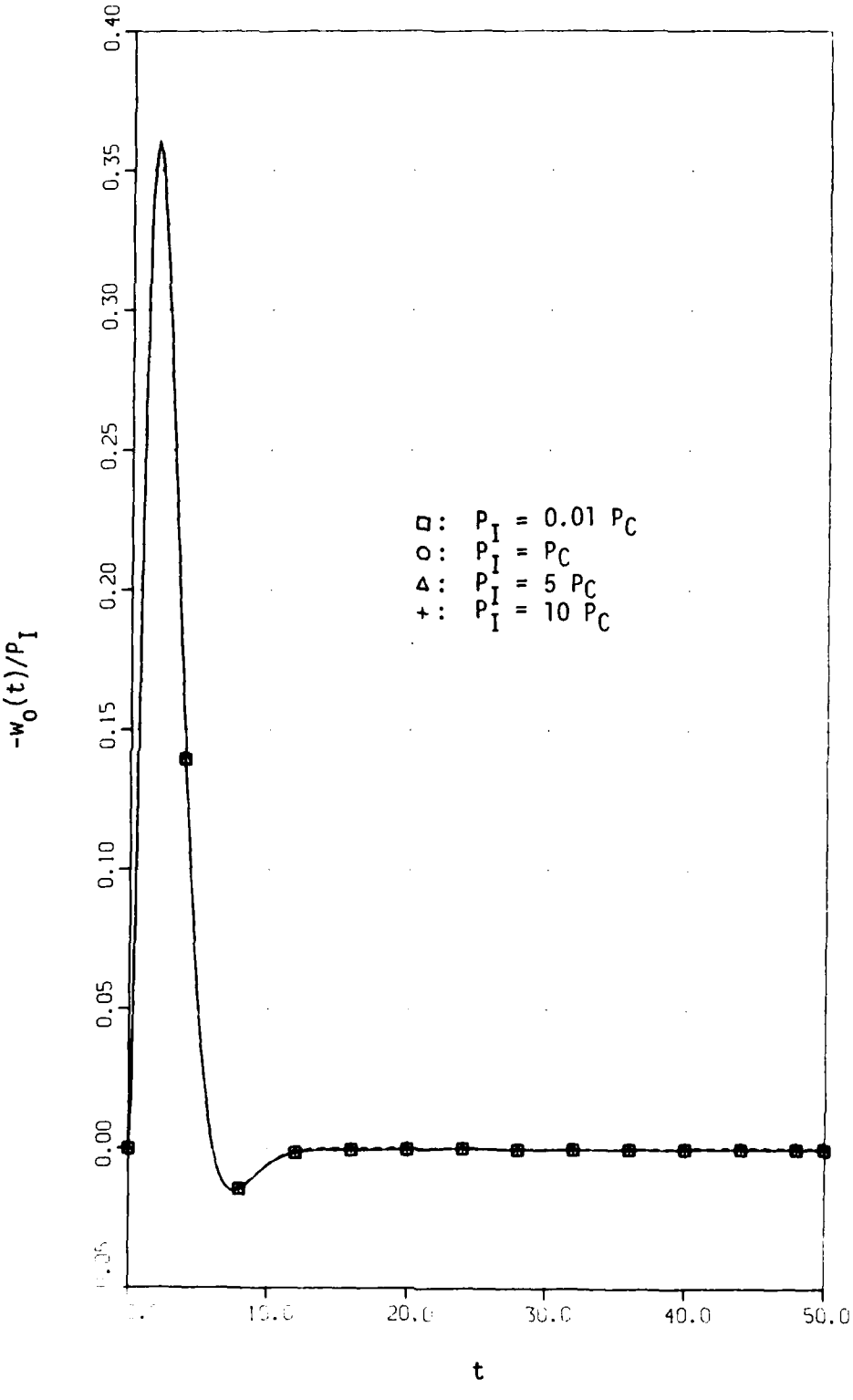

FIGURE 6. n=0 Displacement Response of the γ = 10 Shell to Exponential Incident Waves with λ = 1.

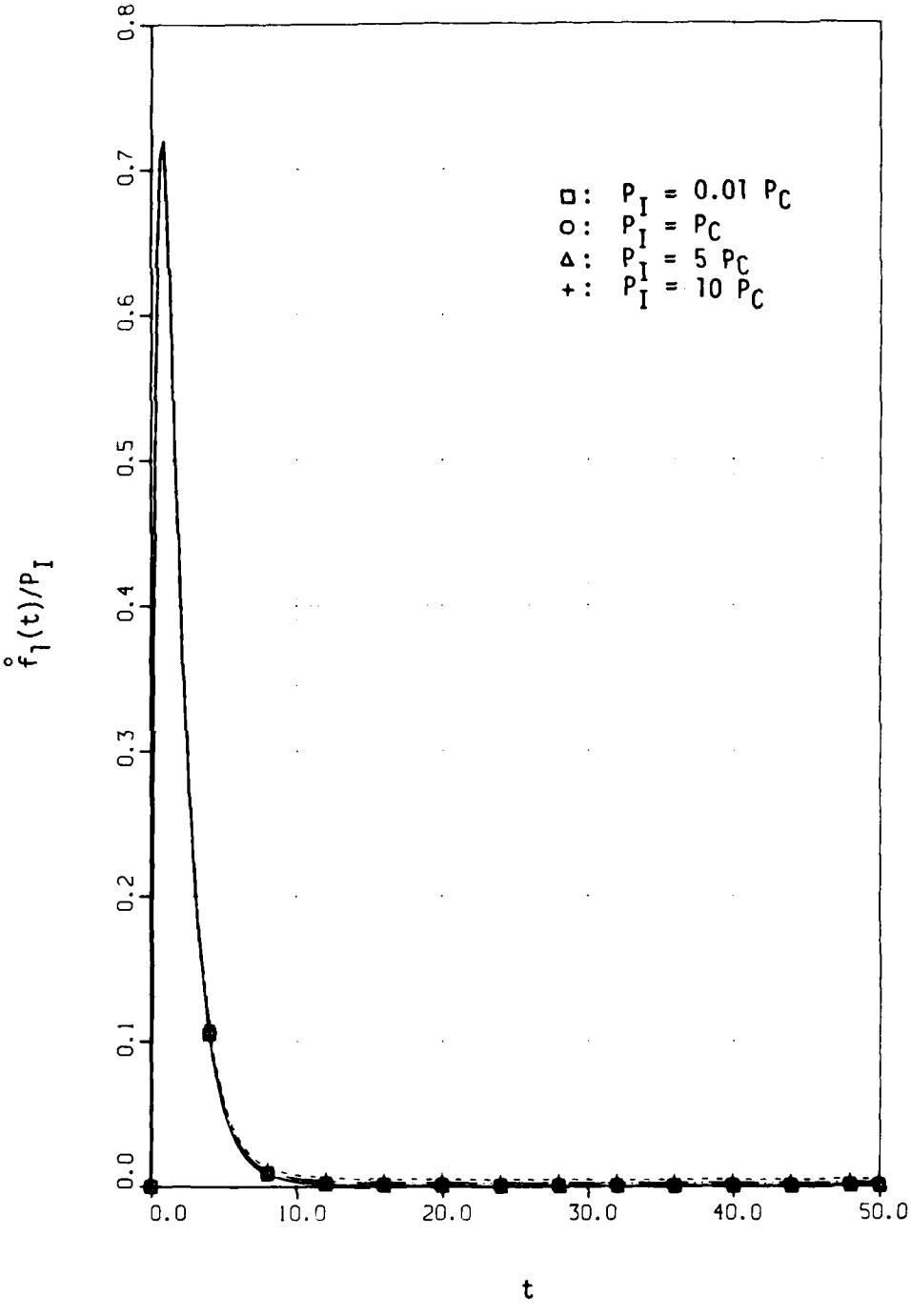

FIGURE 7. n=1 Velocity Response of the $\gamma = 10$ Shell to Exponential Incident Waves with $\lambda = 1$.

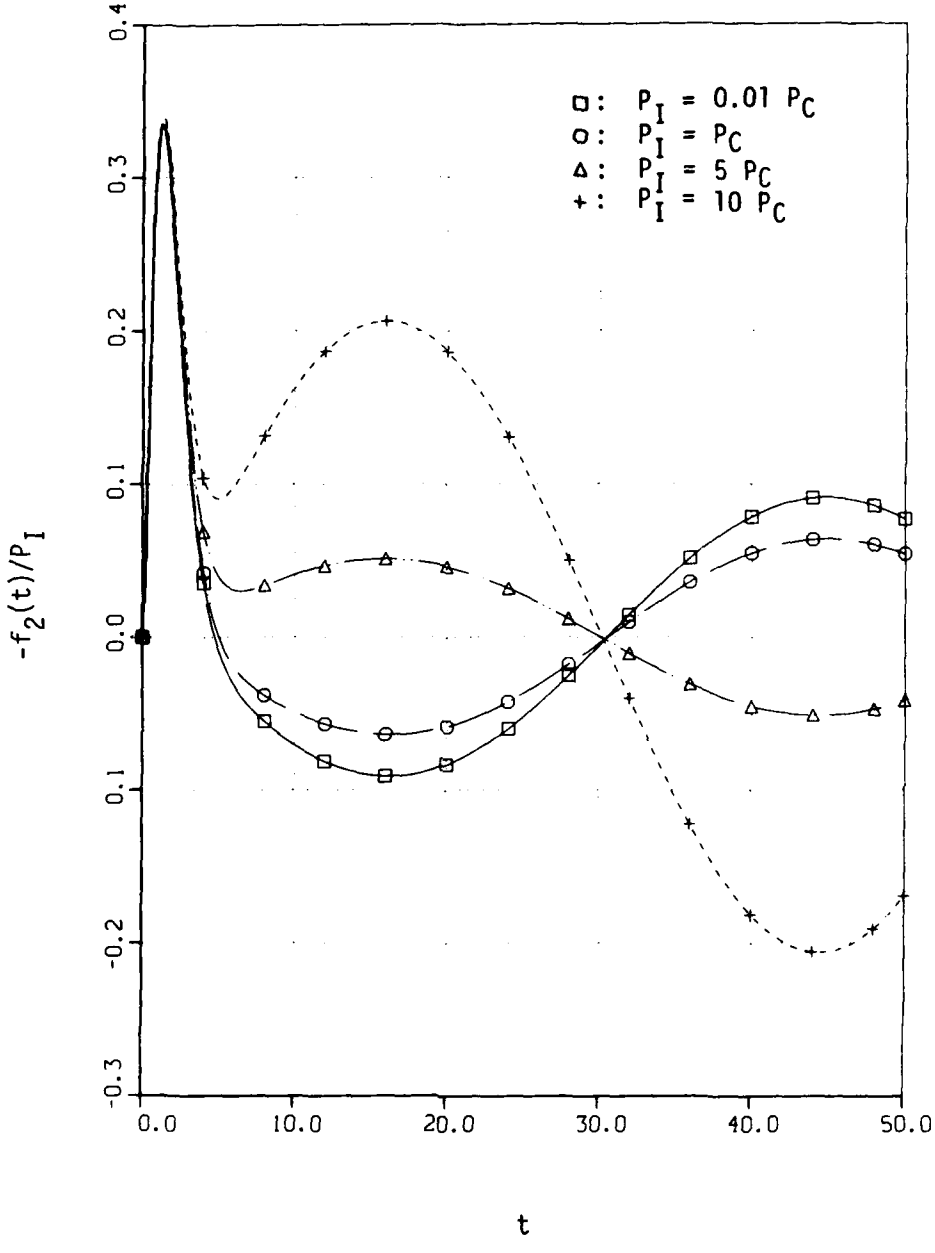

FIGURE 8. n=2 Displacement Response of the $\gamma = 10$ Shell to Exponential Incident Waves with $\lambda = 1$.

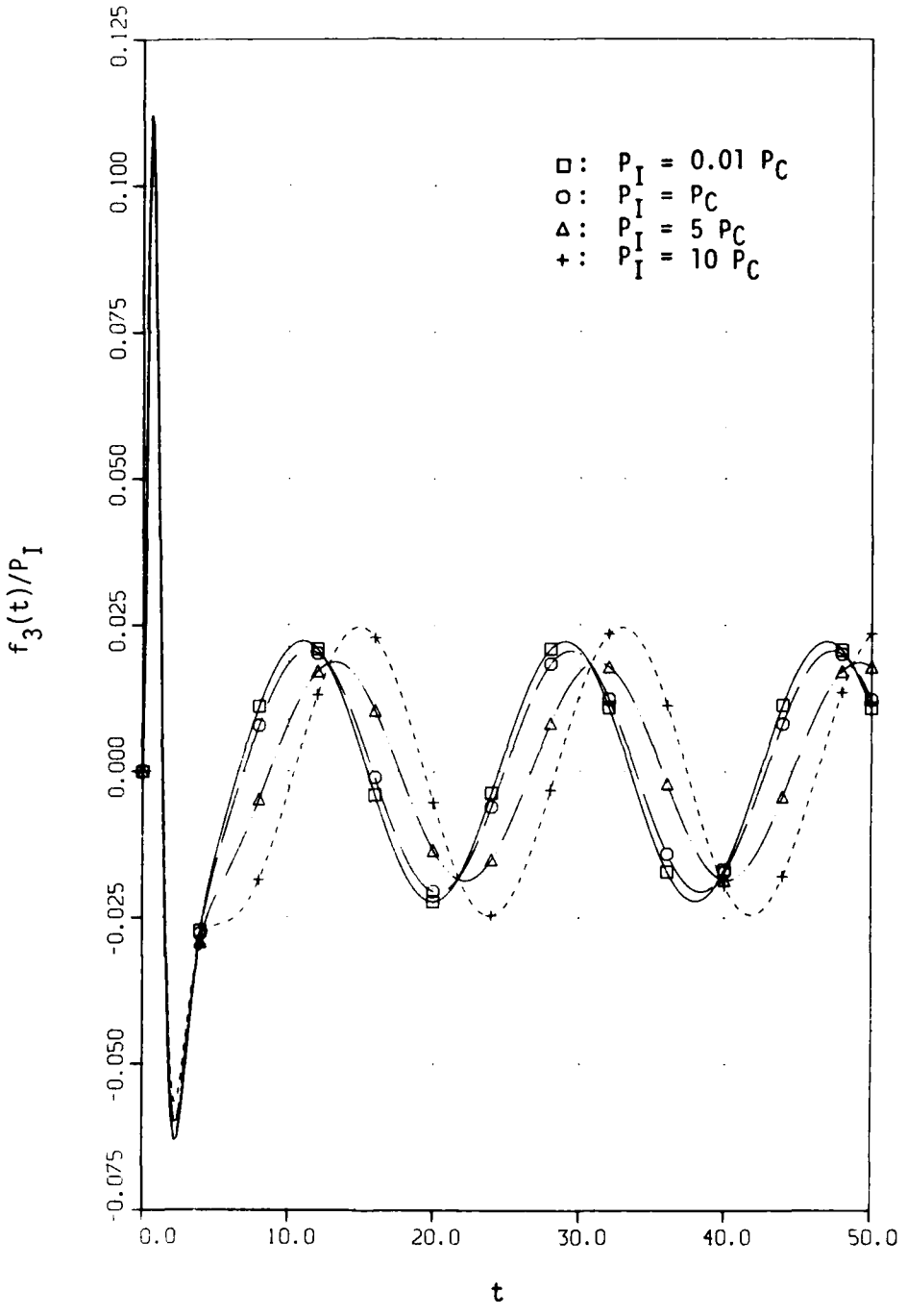

FIGURE 9. n=3 Displacement Response of the $\gamma = 10$ Shell to Exponential Incident Waves with $\lambda = 1$.

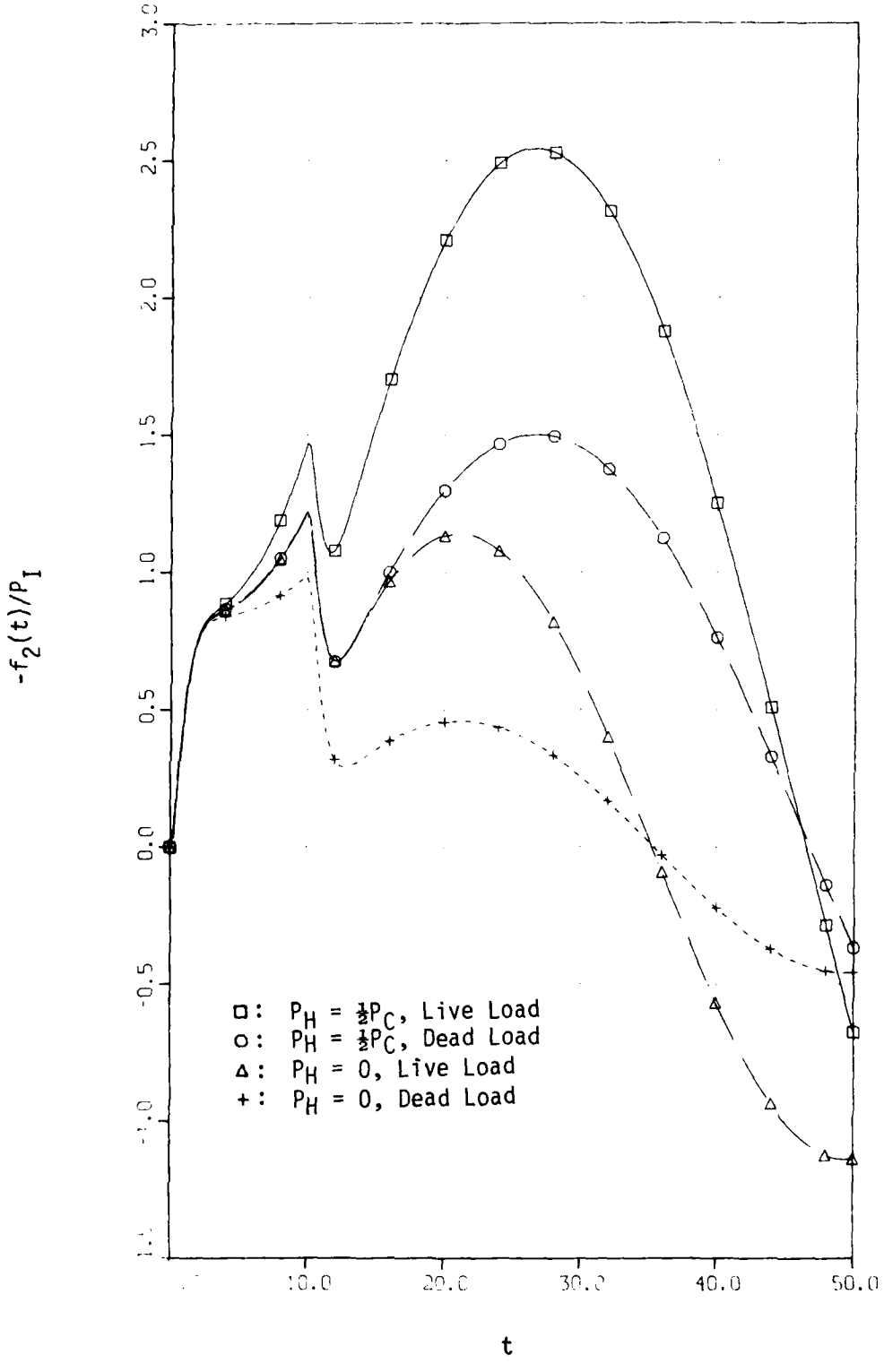

FIGURE 10. n=3 Displacement Response of the $\gamma = 10$ Shell to a Rectangular Incident Wave with $T = 10$, $P_I = 2P_C$.

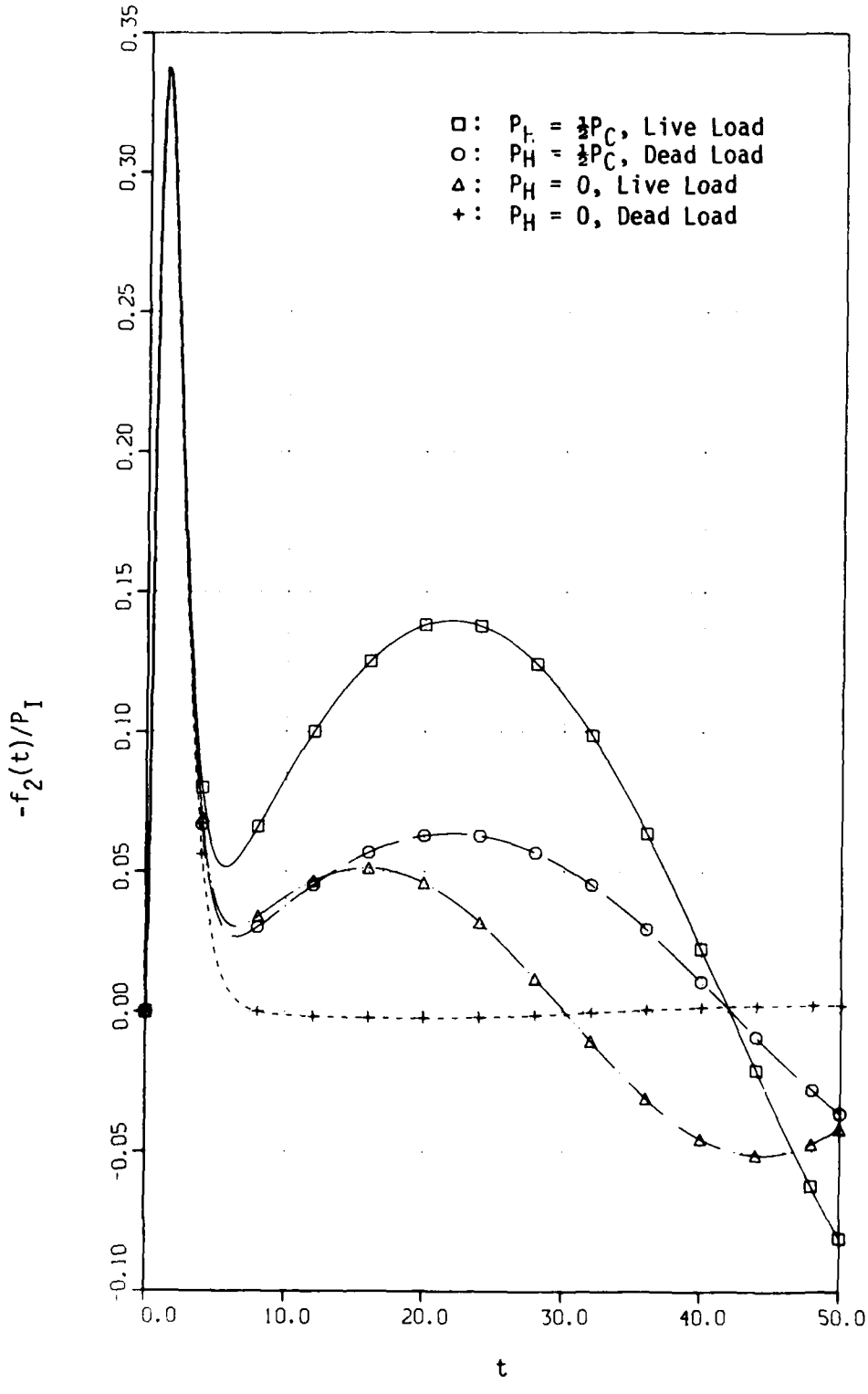

FIGURE 11. n=2 Displacement Response of the $\gamma = 10$ Shell to an Exponential Incident Wave with $\lambda = 1$, $P_I = 5P_C$.

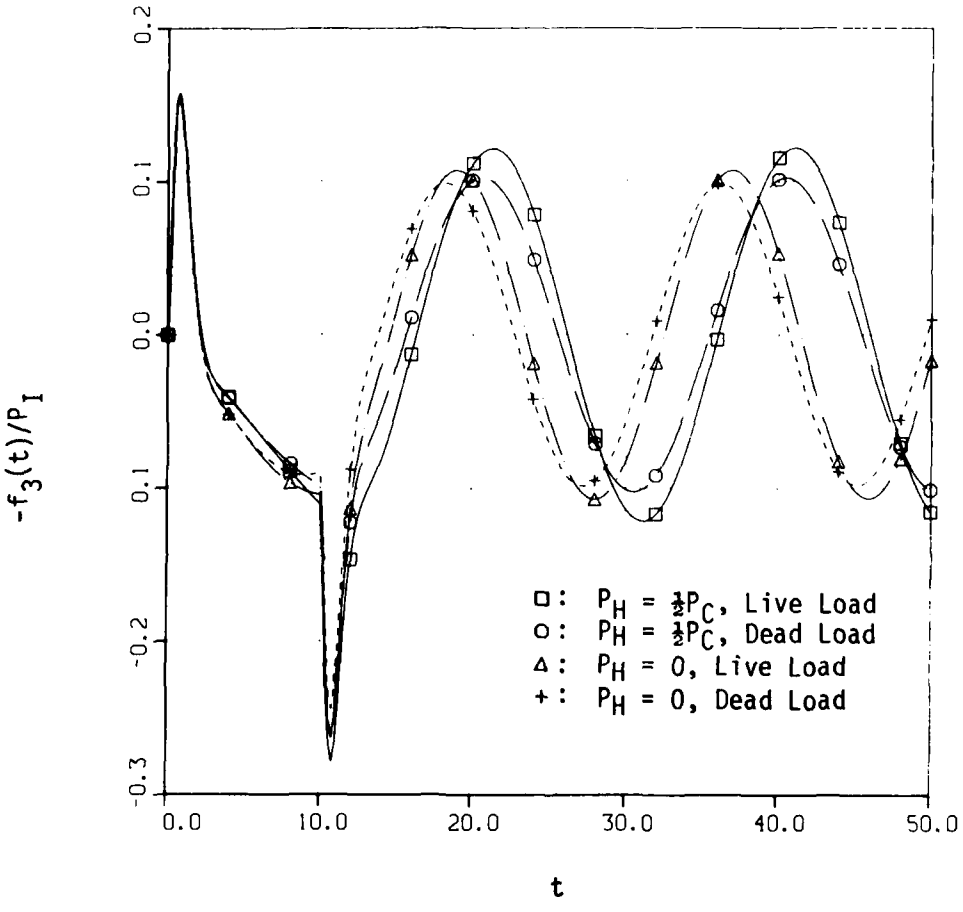

FIGURE 12. n=3 Displacement Response of the $\gamma = 10$ Shell to a Rectangular Incident Wave with $T = 10$, $P_I = 2P_C$.

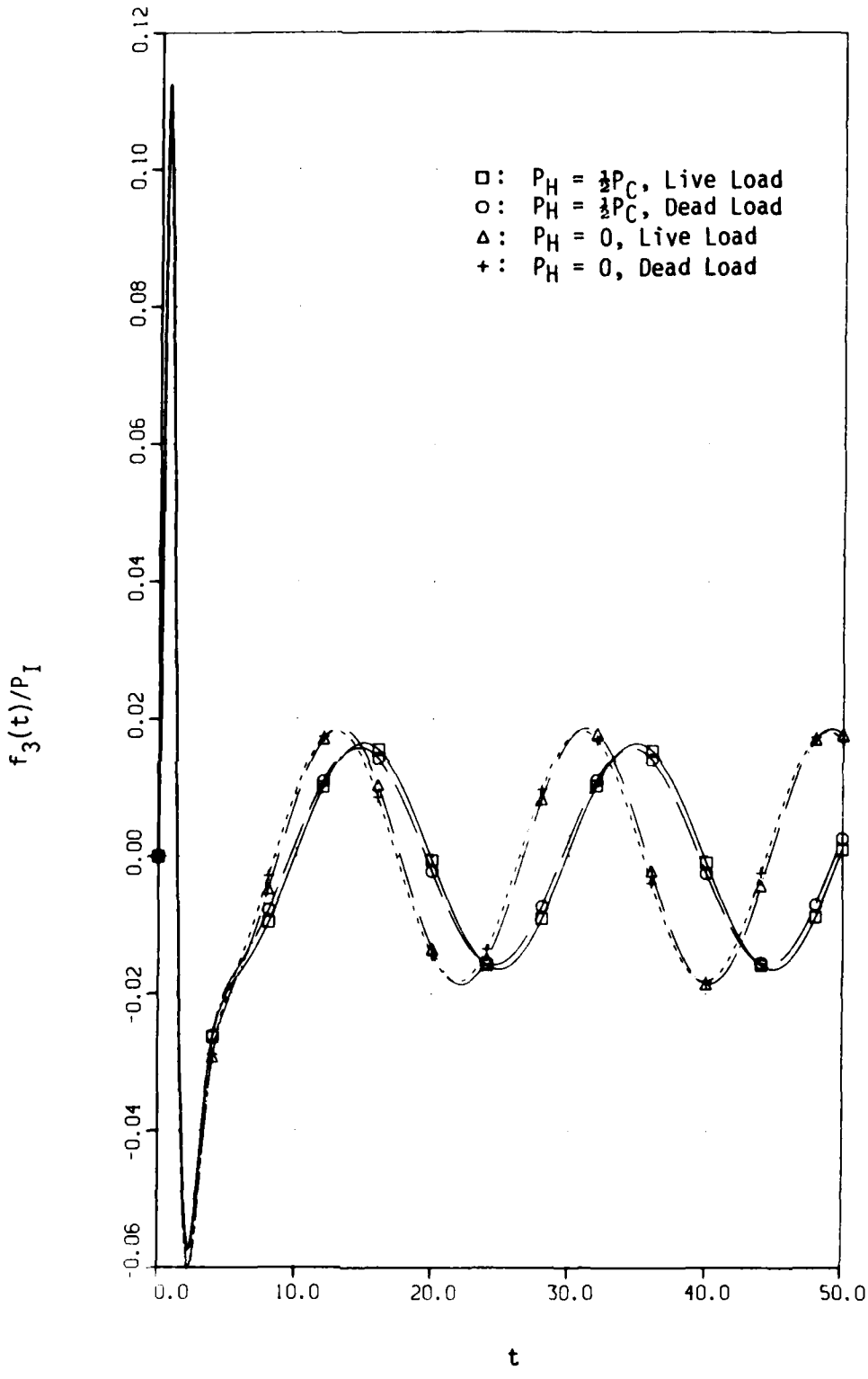

FIGURE 13. n=3 Displacement Response of the $\gamma = 10$ Shell to an Exponential Incident Wave with $\lambda = 1$, $P_I = 5P_C$.

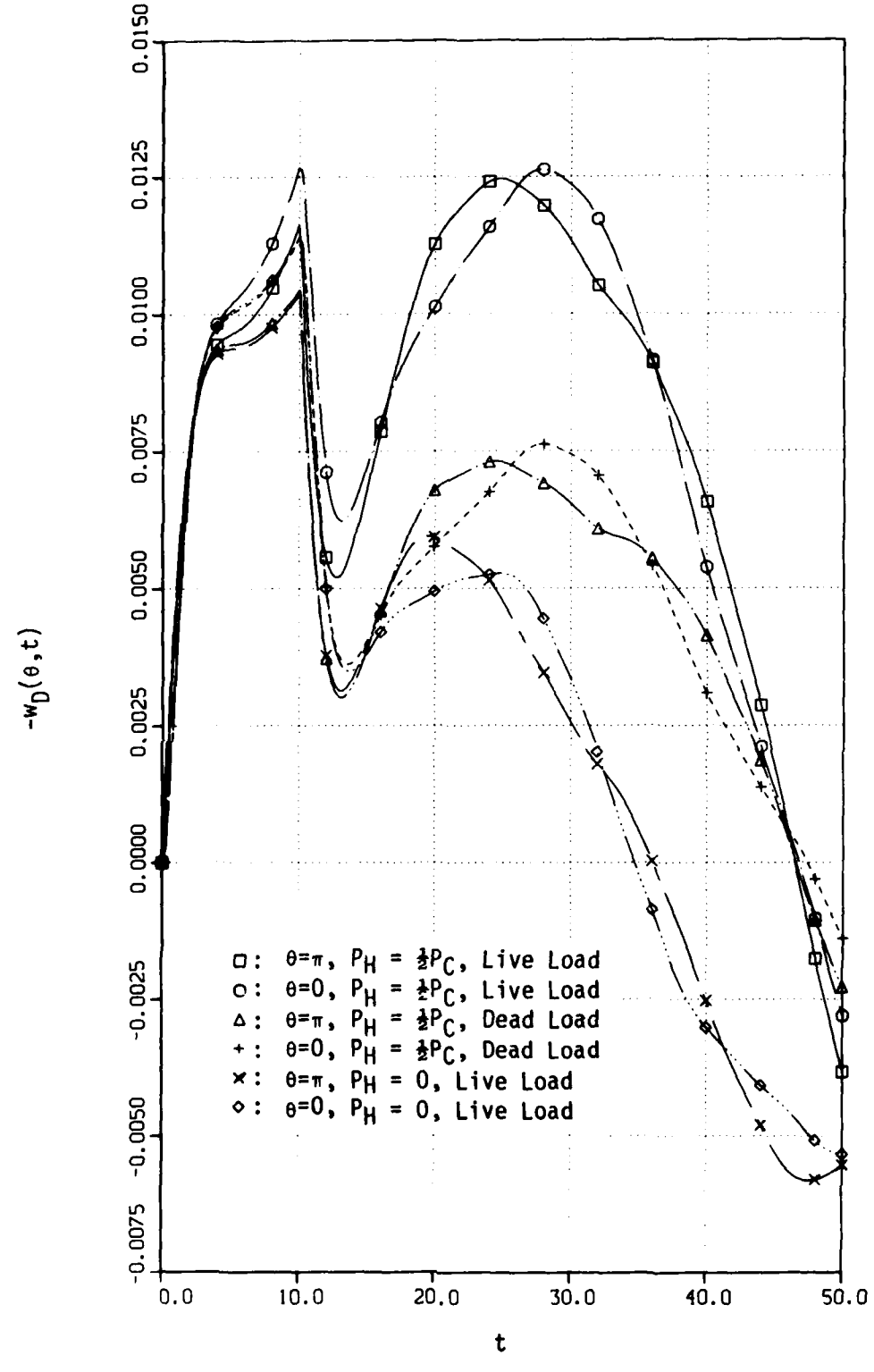

FIGURE 14. Deformational Displacement Response of the γ = 10 Shell to a Rectangular Incident Wave with T = 10, $P_I = 2P_C$.

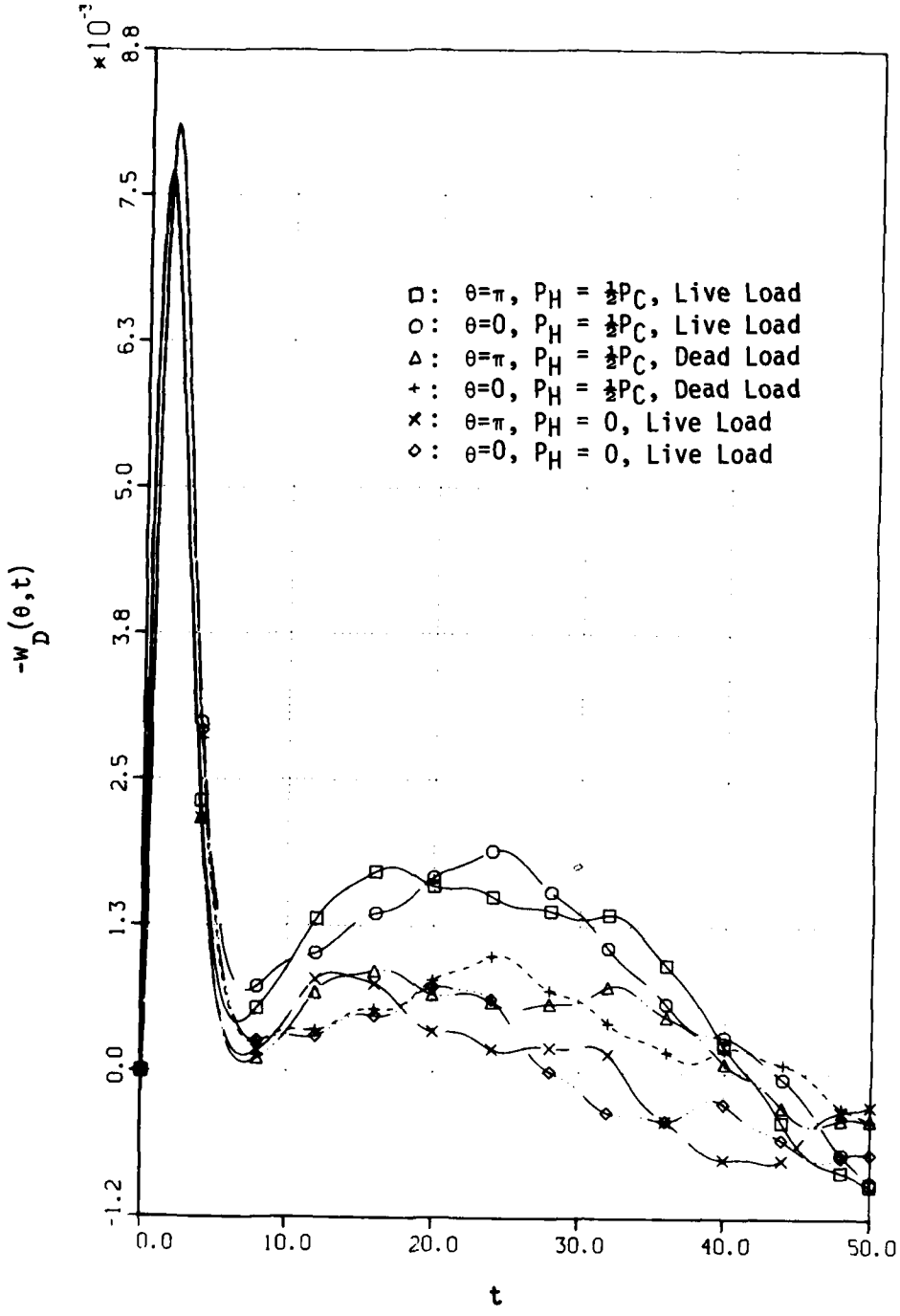

FIGURE 15. Deformational Displacement Response of the $\gamma = 10$ Shell to an Exponential Incident Wave with $\lambda = 1$, $P_I = 5P_C$.

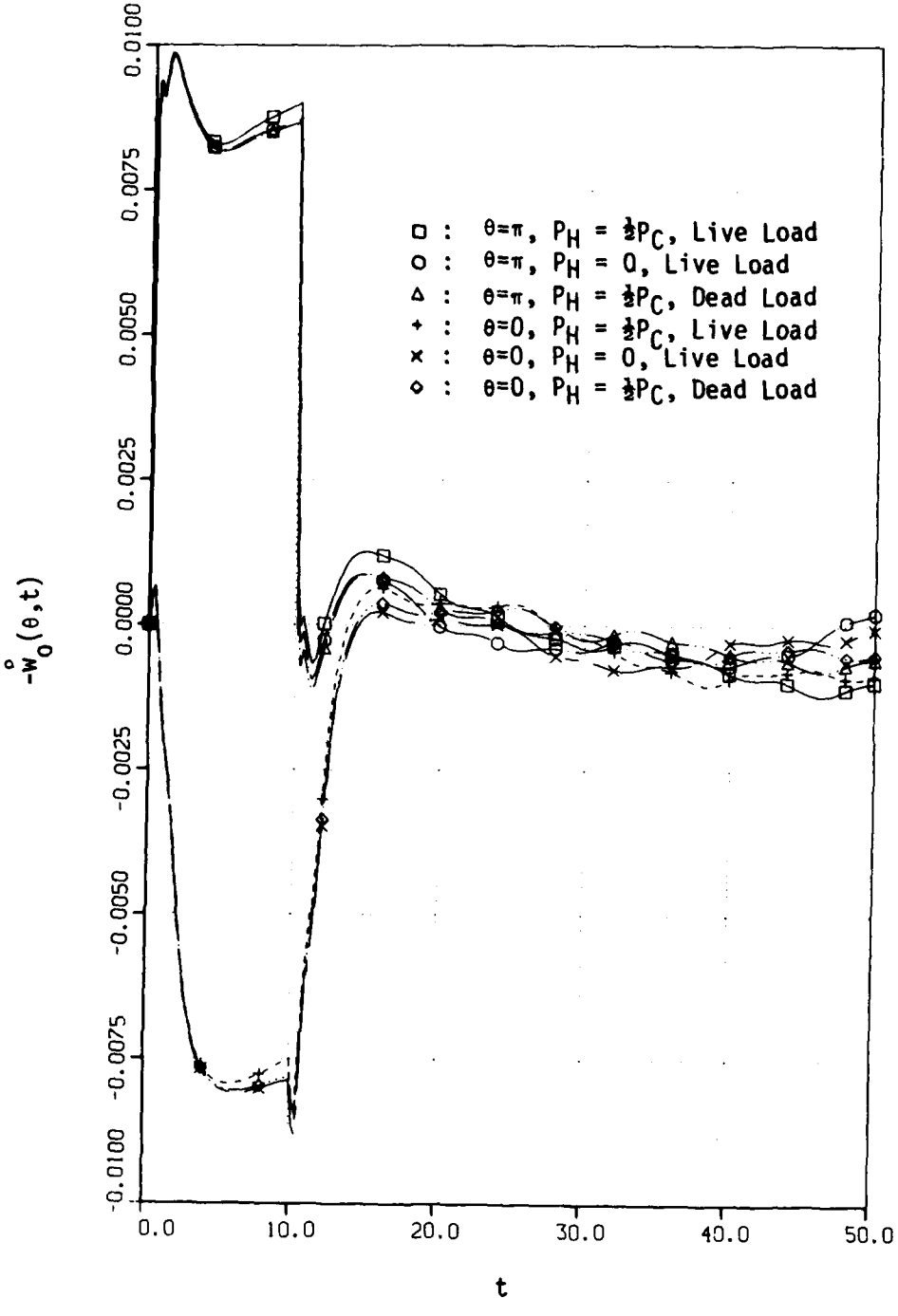

FIGURE 16. Radial Velocity Response of the $\gamma = 10$ Shell to a Rectangular Incident Wave with $T = 10$, $P_I = 2P_C$.

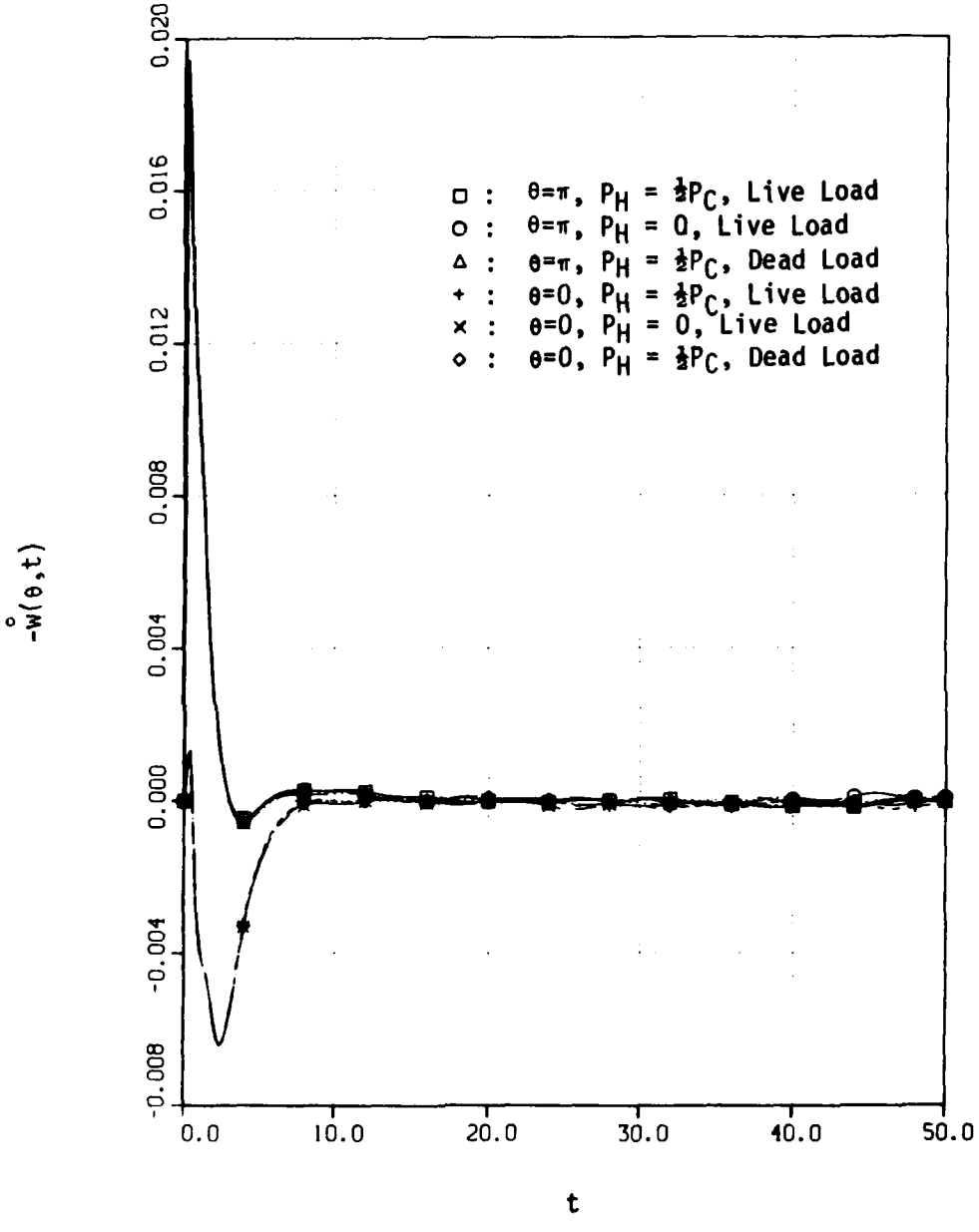

FIGURE 17. Radial Velocity Response of the γ = 10 Shell to an Exponential Incident Wave with λ = 1, $P_I = 5P_C$.

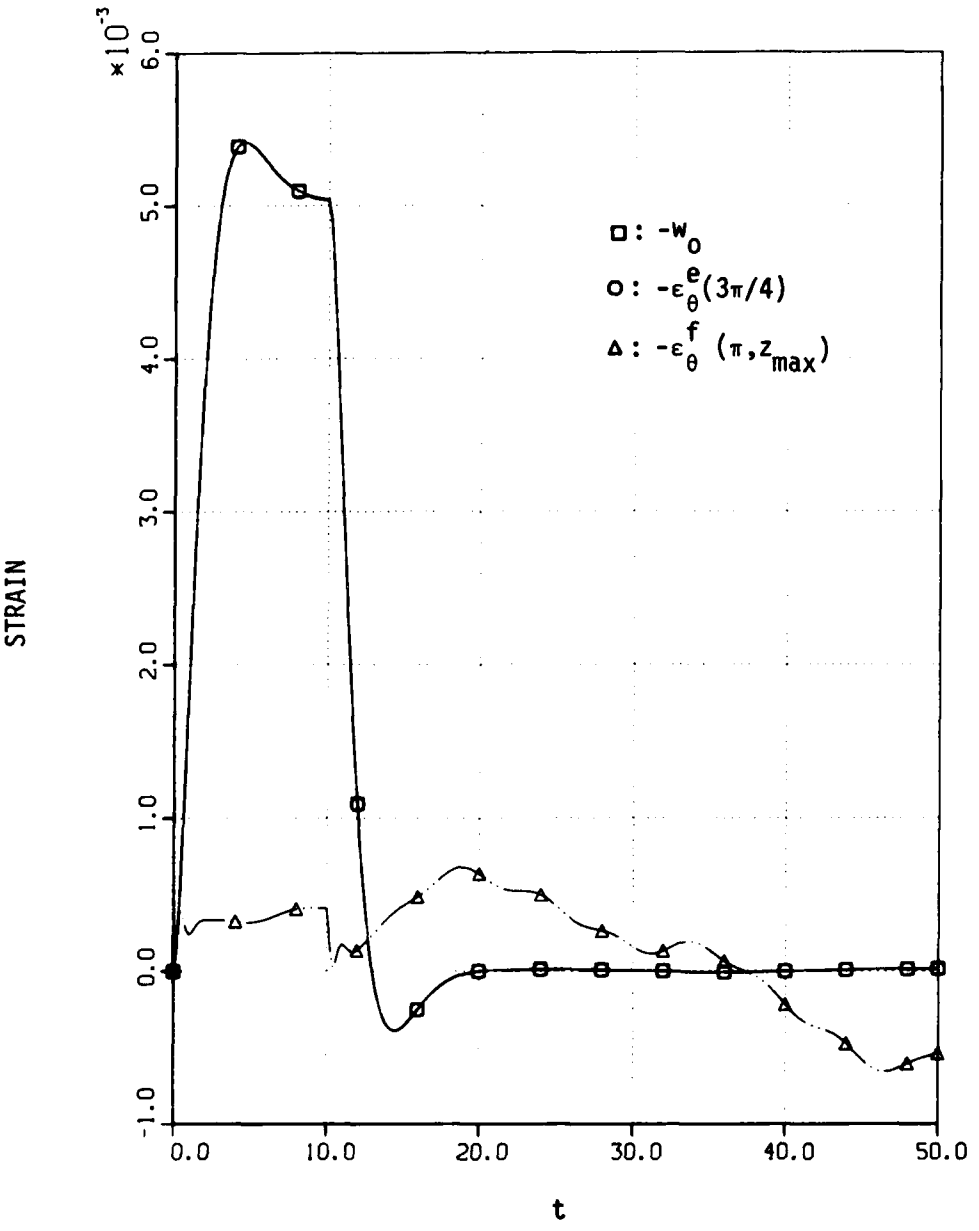

FIGURE 18. Strain Response of the $\gamma = 10$ Shell to a Rectangular Incident Wave with $T = 10$, $P_I = 2P_C$.

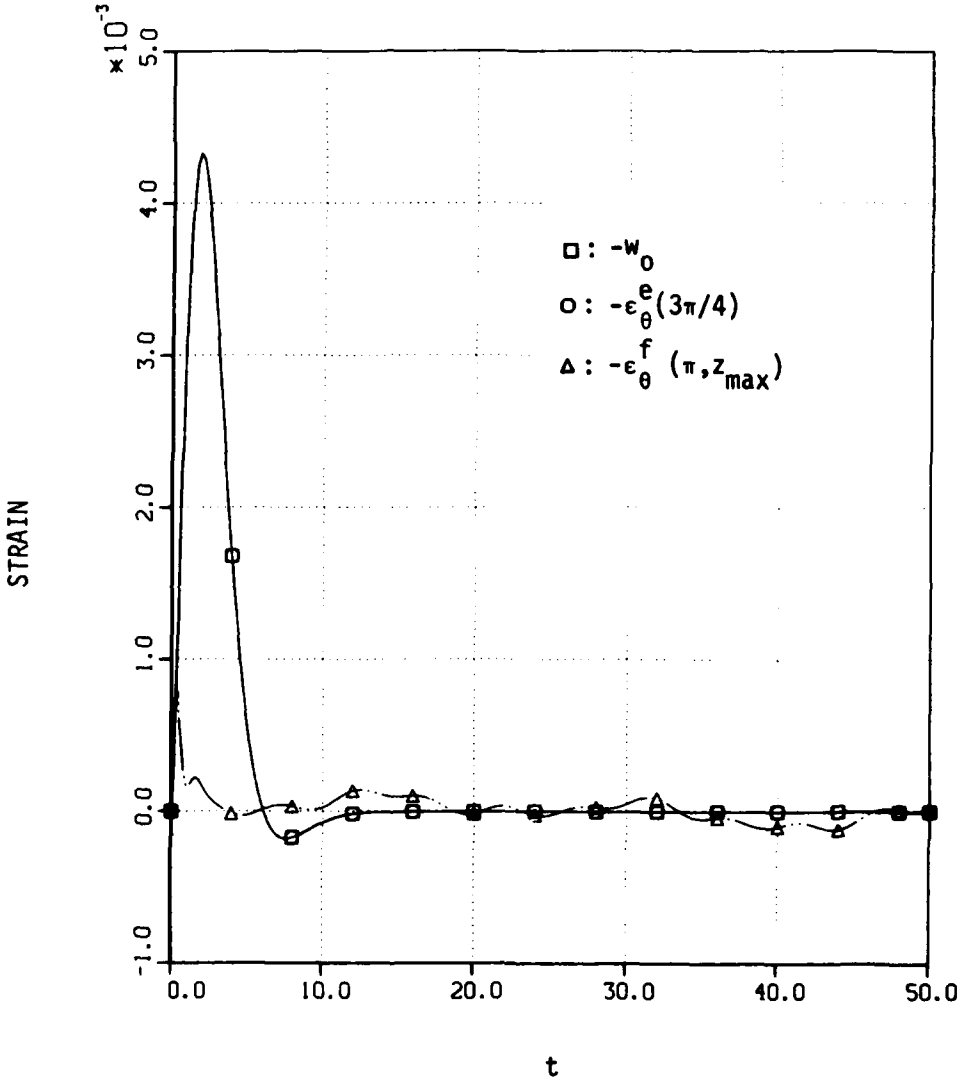

FIGURE 19. Strain Response of the $\gamma = 10$ Shell to an Exponential Incident Wave with $\lambda = 1$, $P_I = 5P_C$.

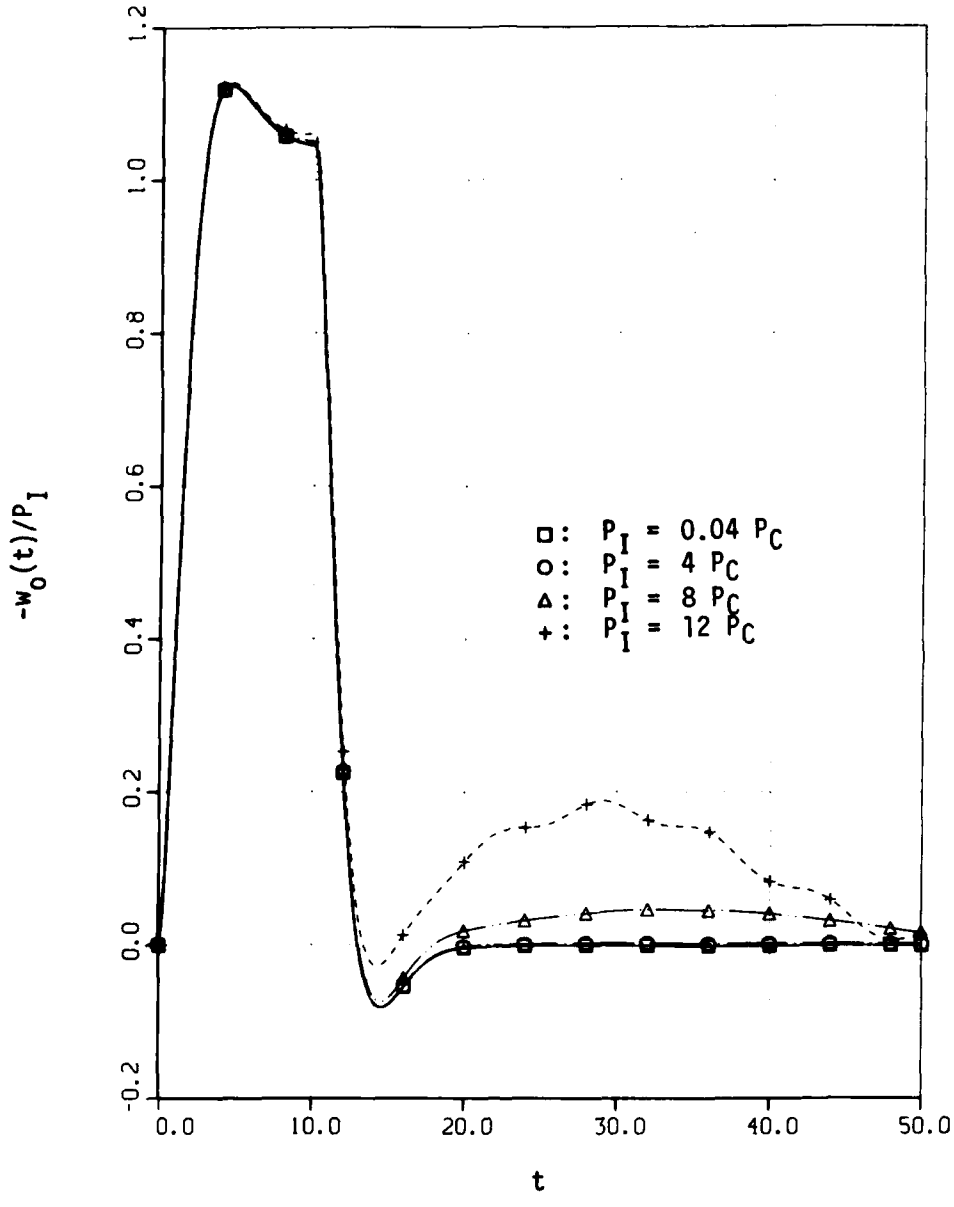

FIGURE 20. n=0 Displacement Response of the γ = 5 Shell to Rectangular Incident Waves with T = 10.

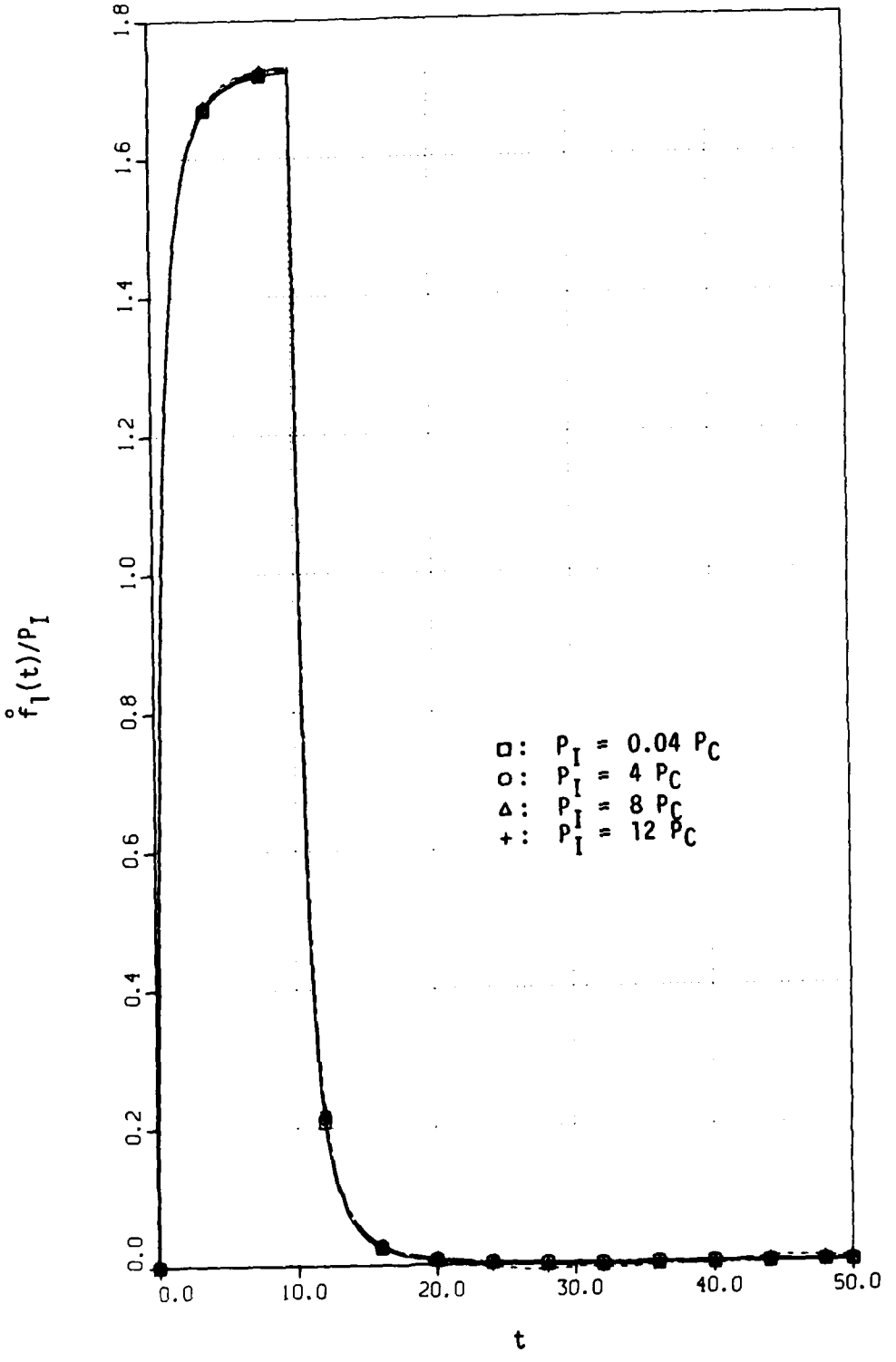

FIGURE 21. n=1 Velocity Response of the γ = 5 Shell to Rectangular Incident Waves with T = 10.

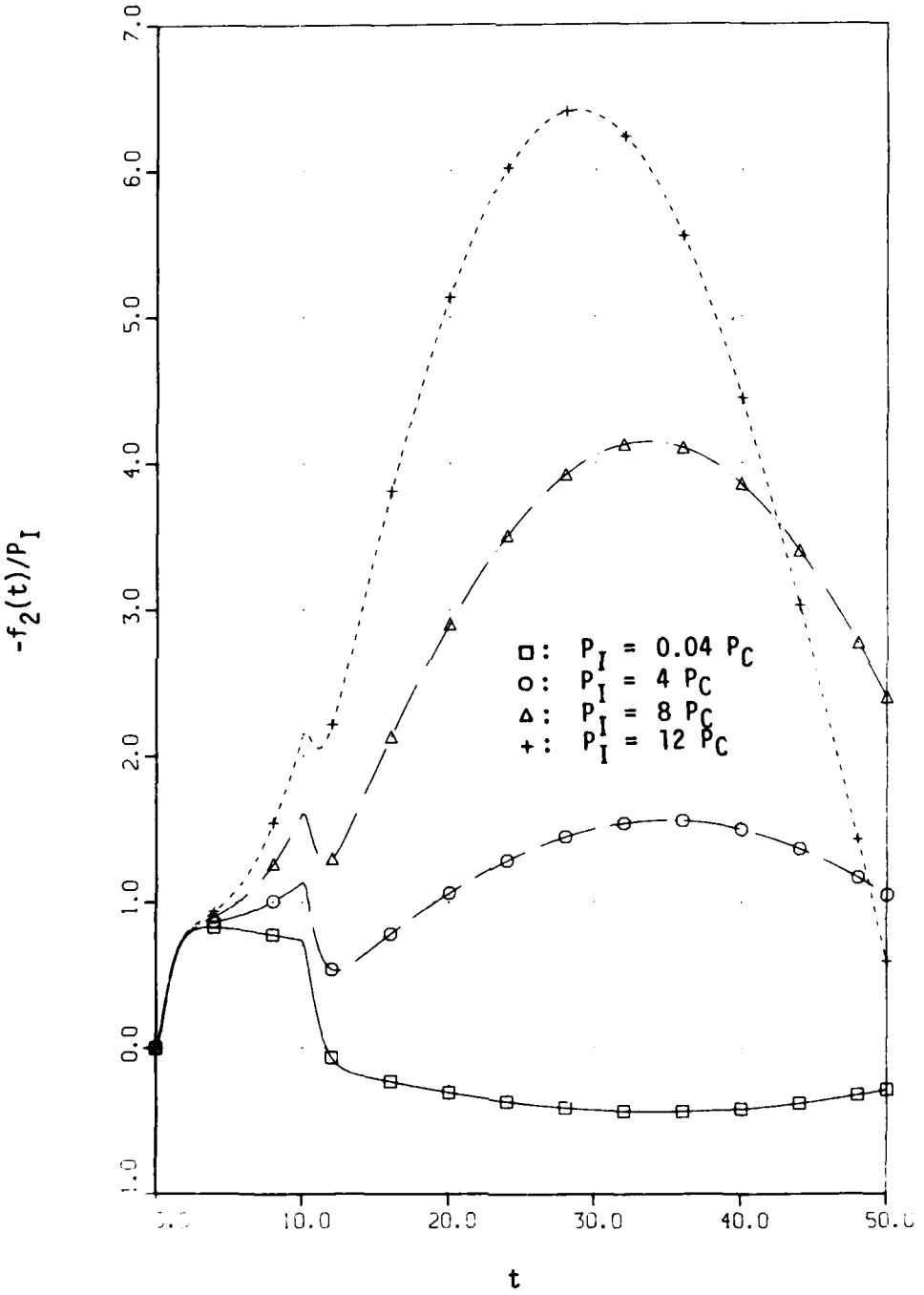

FIGURE 22. n=2 Displacement Response of the γ = 5 Shell to Rectangular Incident Waves with T = 10.

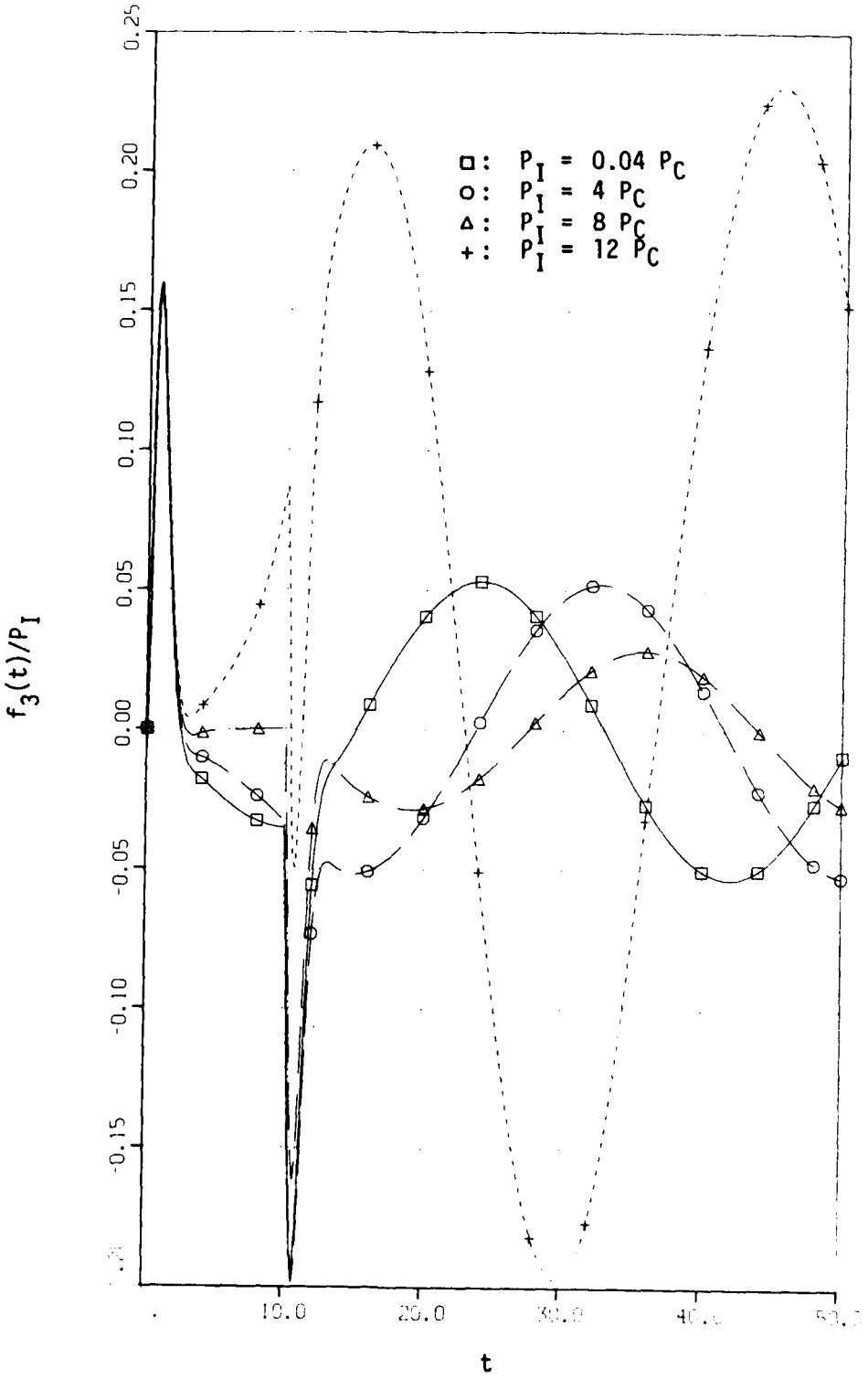

FIGURE 23. n=3 Displacement Response of γ = 5 Shell to Rectangular Incident Waves with T = 10.

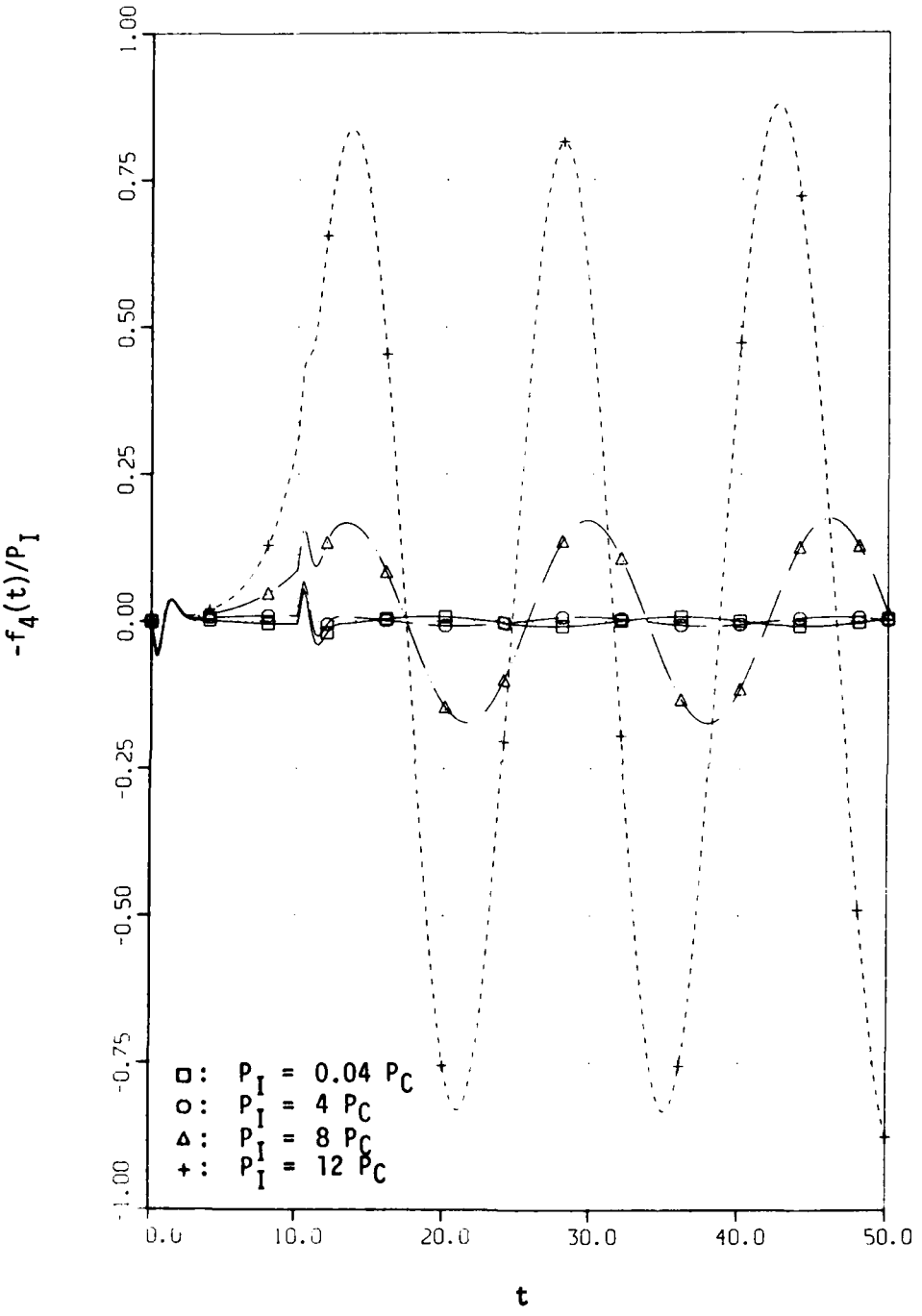

FIGURE 24. n=4 Displacement Response of the γ = 5 Shell to Rectangular Incident Waves with T = 10.

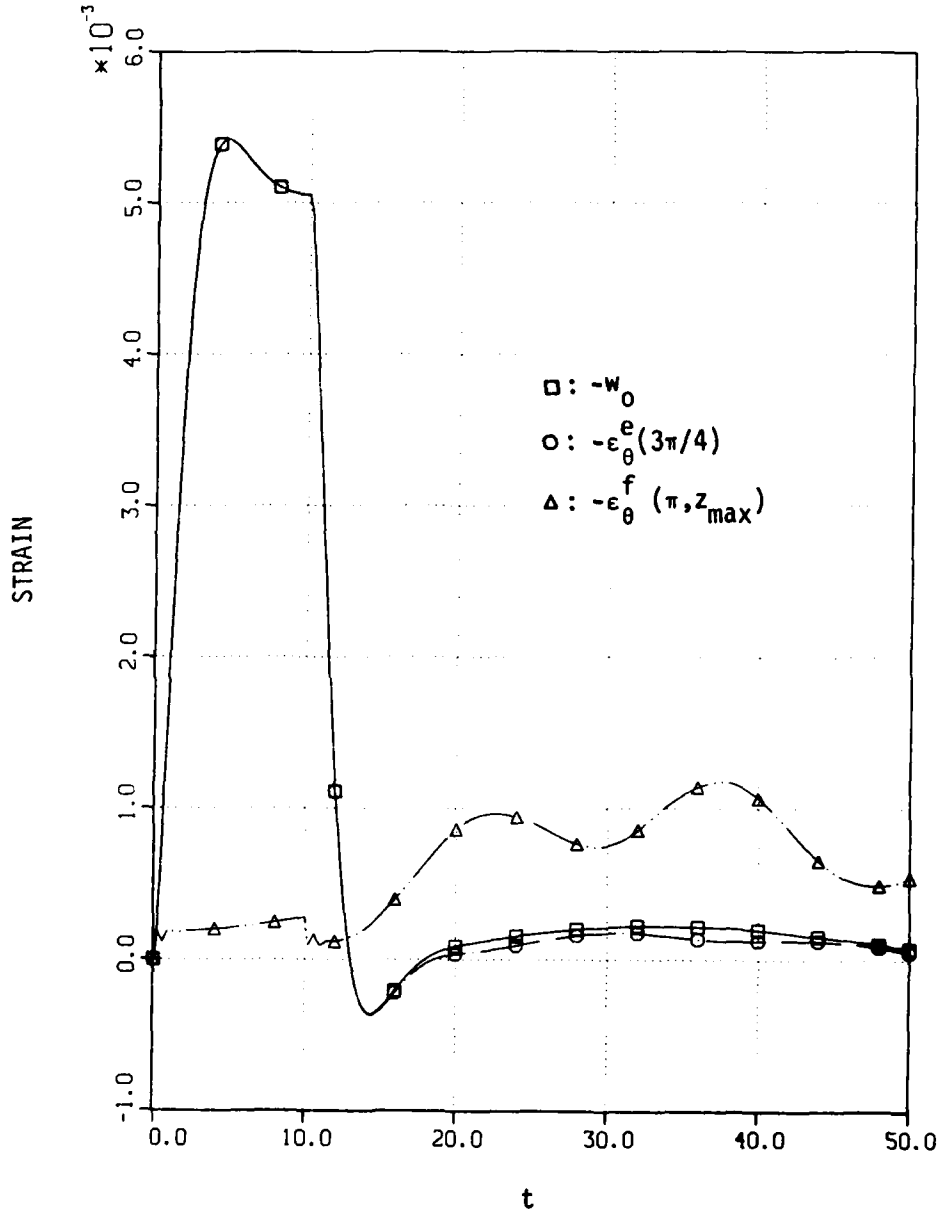

FIGURE 25. Strain Response of the $\gamma = 5$ Shell to a Rectangular Incident Wave with $T = 10$, $P_I = 8P_C$.

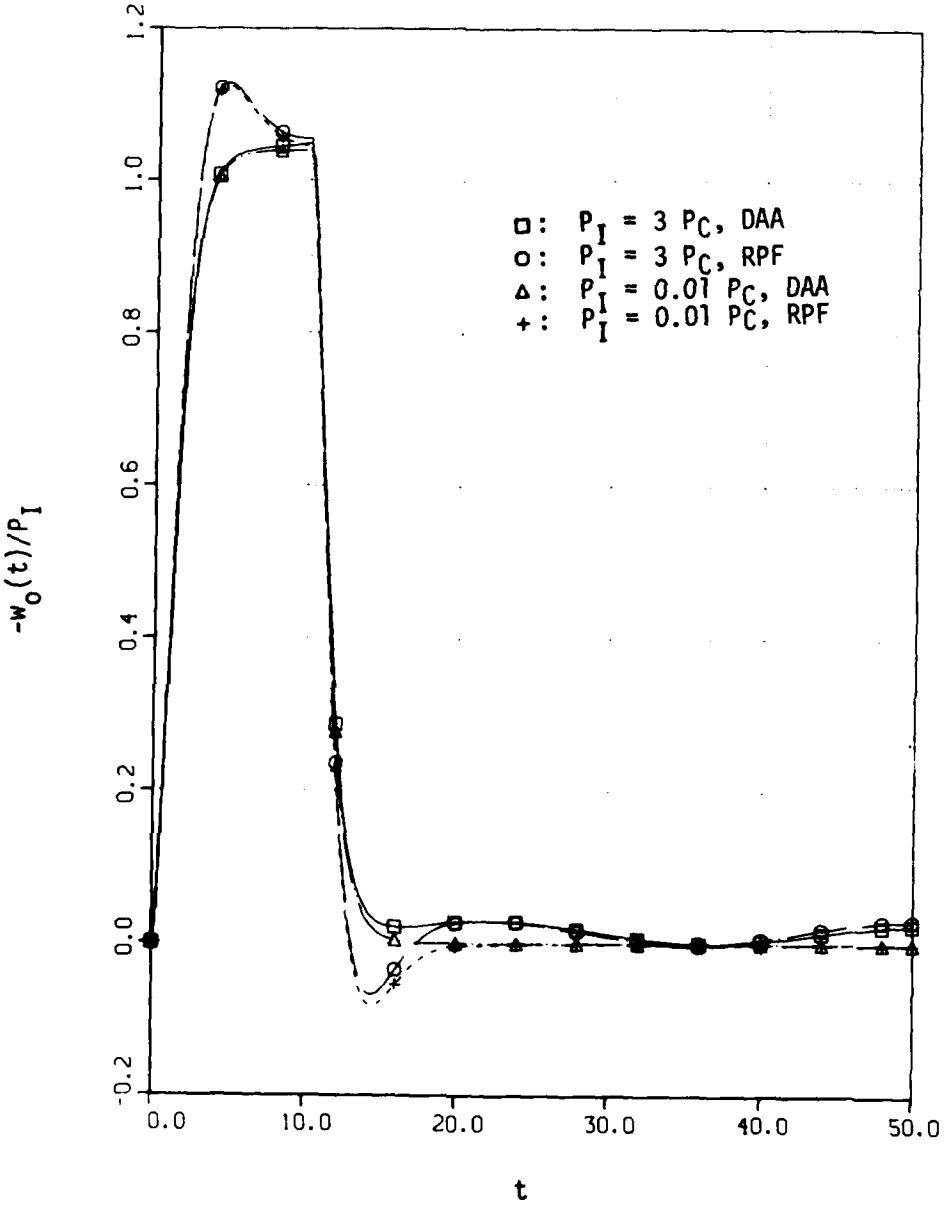

FIGURE 26. Approximate and Exact n=0 Displacement Response of the γ = 10 Shell to Rectangular Incident Waves with T = 10.

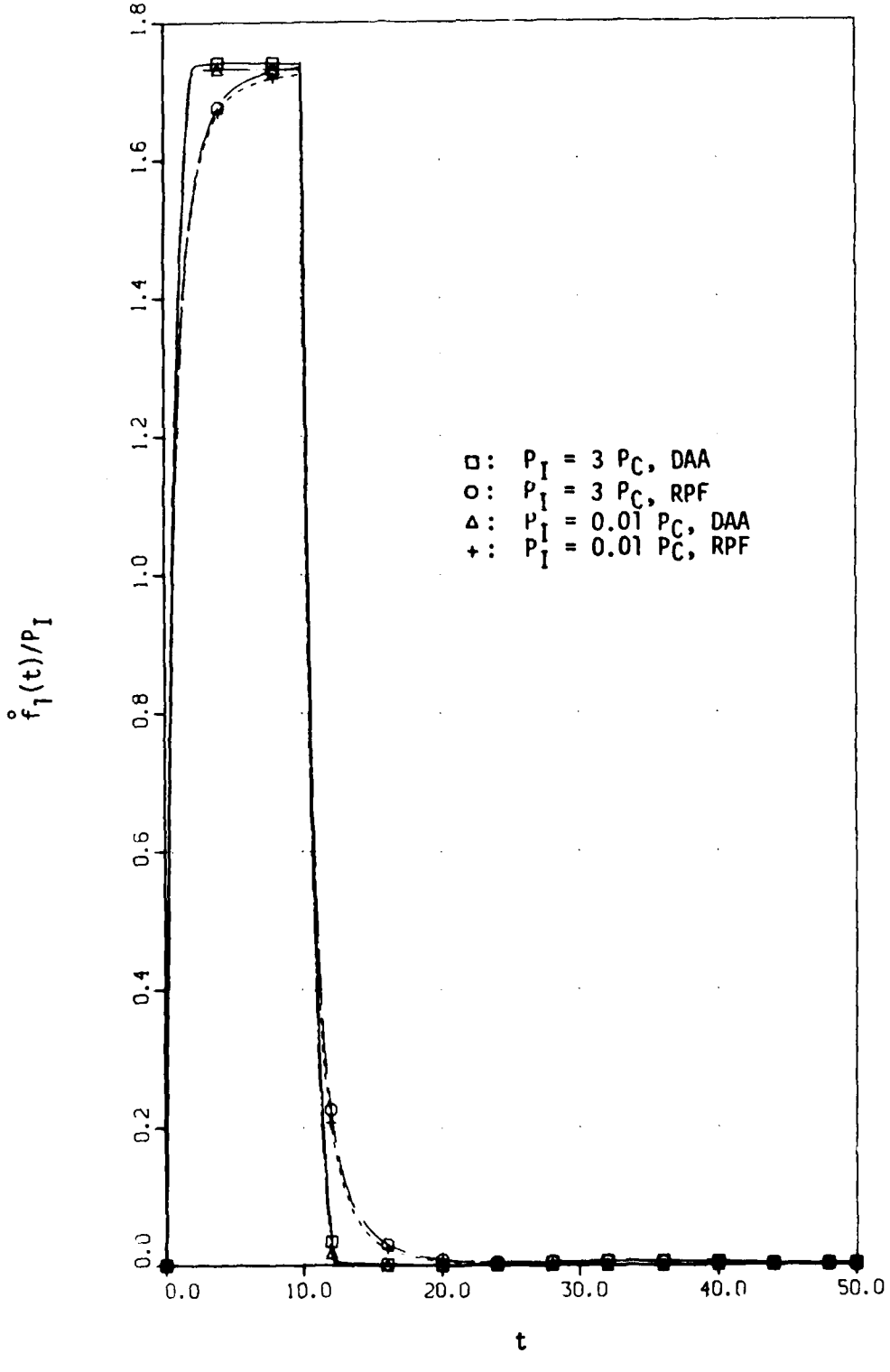

FIGURE 27. Approximate and Exact n=1 Velocity Response of the γ = 10 Shell to Rectangular Incident Waves with T = 10.

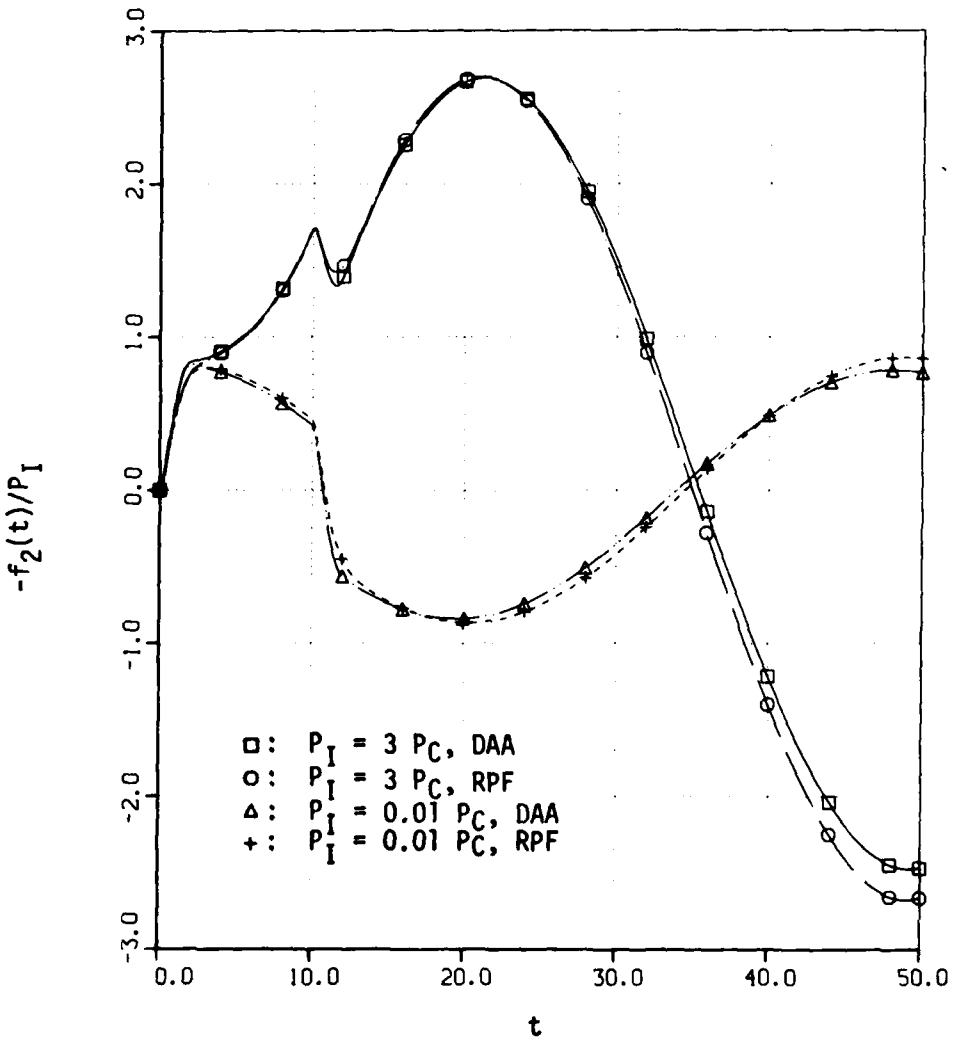

FIGURE 28. Approximate and Exact n=2 Displacement Response of the γ = 10 Shell to Rectangular Incident Waves with T = 10.

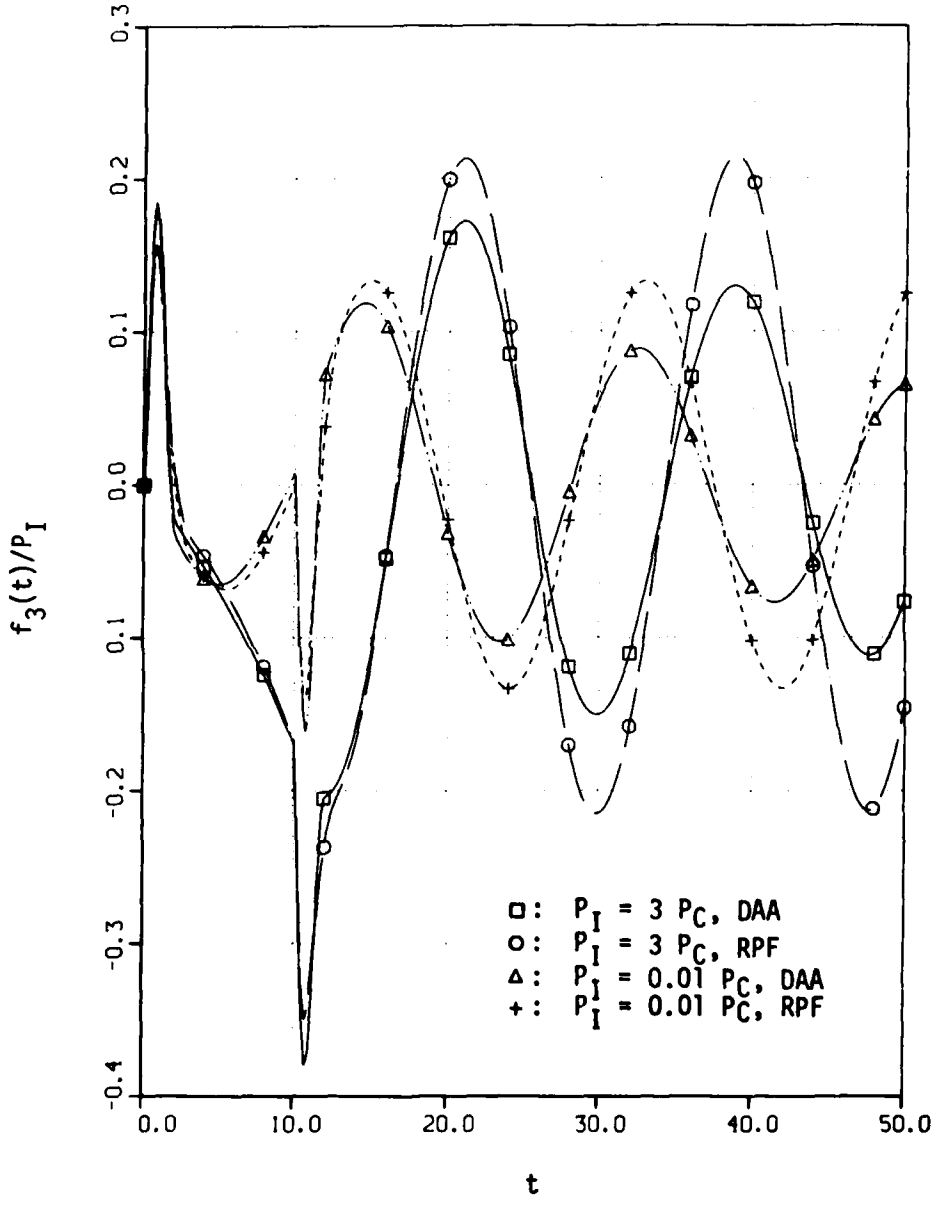

FIGURE 29. Approximate and Exact n=3 Displacement Response of the γ = 10 Shell to Rectangular Incident Waves with T = 10.

DISTRIBUTION LIST

DEPARTMENT OF DEFENSE

Defense Advanced Rsch. Proj. Agency
ATTN: TIO

Defense Technical Information Center
12 cy ATTN: DD

Defense Intelligence Agency
ATTN: RDS-3A
ATTN: DT-2
ATTN: DT-1C
ATTN: DB-4C

Defense Nuclear Agency
ATTN: DDST
4 cy ATTN: TITL
2 cy ATTN: SPSS

Field Command
Defense Nuclear Agency
ATTN: FCPR

Field Command
Defense Nuclear Agency
Livermore Division
ATTN: FCPRL

Interservice Nuclear Weapons School
ATTN: TTV

Undersecretary of Def. for Rsch. & Engrg.
ATTN: Strategic & Space Systems (OS)

DEPARTMENT OF THE ARMY

Deputy Chief of Staff for Rsch. Dev. & Acq.
Department of the Army
ATTN: DAMA-CSS-N

Harry Diamond Laboratories
Department of the Army
ATTN: DELHD-I-TL
ATTN: DELHD-N-P

U.S. Army Ballistic Research Labs
ATTN: DRDAR-TSB-S

U.S. Army Engr. Waterways Exper. Station
ATTN: Library

U.S. Army Material & Mechanics Rsch. Ctr.
ATTN: DRXMR-TE, R. Shea

U.S. Army Nuclear & Chemical Agency
ATTN: Library

DEPARTMENT OF THE NAVY

Naval Construction Battalion Center
Civil Engineering Laboratory
ATTN: Code L08A

Naval Electronic Systems Command
ATTN: PME 117-21

DEPARTMENT OF THE NAVY (Continued)

David Taylor Naval Ship R & D Ctr.
ATTN: Code 1740.1
ATTN: Code 173
ATTN: Code 1844
ATTN: Code 1740.6
ATTN: Code L42-3
ATTN: Code 11
ATTN: Code 172
ATTN: Code 2740
2 cy ATTN: Code 1770.1
2 cy ATTN: Code 1740.5

Naval Facilities Engineering Command
ATTN: Code 09M22C

Naval Material Command
ATTN: MAT 08T-22

Naval Ocean Systems Center
ATTN: Code 4471

Naval Postgraduate School
ATTN: Code 0142
ATTN: Code 69NE

Naval Research Laboratory
ATTN: Code 8003
ATTN: Code 8301
ATTN: Code 6380
ATTN: Code 8100
ATTN: Code 8406
ATTN: Code 8445
ATTN: Code 2627
ATTN: Code 8440

Naval Sea Systems Command
ATTN: SEA-09G53
2 cy ATTN: SEA-3221
2 cy ATTN: SEA-08
2 cy ATTN: SEA-323

Naval Surface Weapons Center
ATTN: Code R13
ATTN: Code F31
ATTN: Code R10
ATTN: Code R15
2 cy ATTN: Code R14

Naval Surface Weapons Center
ATTN: Tech. Library & Info. Services Branch

Naval Weapons Center
ATTN: Code 233

Naval Weapons Evaluation Facility
ATTN: Code 10

New London Laboratory
Naval Underwater Systems Center
ATTN: Code 401, J. Kalinowski
ATTN: Code 401, J. Patel

DEPARTMENT OF THE NAVY (Continued)

Newport Laboratory
Naval Underwater Systems Center
ATTN: Code EM
ATTN: *Code 363, P. Paranzino*

Office of Naval Research
ATTN: Code 715
2 cy ATTN: Code 474, N. Perrone

Office of the Chief of Naval Operations
ATTN: OP 982
ATTN: OP 953
ATTN: OP 981N1
ATTN: OP 957E
ATTN: OP 951
ATTN: OP 37
ATTN: OP 604C
ATTN: OP 03EG
ATTN: OP 987
ATTN: OP 21

Strategic Systems Project Office
Department of the Navy
ATTN: NSP-272
ATTN: NSP-43

DEPARTMENT OF THE AIR FORCE

Air Force Institute of Technology
Air University
ATTN: Library

Air Force Weapons Laboratory, AFSC
ATTN: SUL

DEPARTMENT OF ENERGY CONTRACTORS

Lawrence Livermore Laboratory
ATTN: *Document Control for Technical*
Information Dept. Library

Los Alamos Scientific Laboratory
ATTN: Document Control for D. Nowlin
ATTN: Document Control for MS 364
(Class. Reports Lib.)

Sandia Laboratories
ATTN: Document Control for 3141

Sandia Laboratories
Livermore Laboratory
ATTN: Document Control for Library &
Security Classification Division

DEPARTMENT OF DEFENSE CONTRACTORS

BDM Corp.
ATTN: T. Neighbors

Bolt Beranek & Newman, Inc.
ATTN: R. Haberman

Cambridge Acoustical Assoc., Inc.
ATTN: M. Junger

General Dynamics Corp.
Electric Boat Division
3 cy ATTN: M. Pakstys

DEPARTMENT OF DEFENSE CONTRACTORS (Continued)

General Electric Company-TEMPO
ATTN: DASIAC

University of Illinois
Consulting Services
ATTN: N. Newmark

Institute for Defense Analyses
ATTN: Classified Library

Kaman AviDyne
ATTN: Library

Kaman Sciences Corp.
ATTN: Library

Lockheed Missiles and Space Co., Inc.
ATTN: Technical Information Center
15 cy ATTN: T. Geers
ATTN: C. Yen

Merritt CASES, Inc.
ATTN: Library

Pacifica Technology
2 cy ATTN: J. Kent

Patel Inteprises, Inc.
ATTN: M. Patel

Physics Applications, Inc.
ATTN: C. Vincent

R & D Associates
ATTN: Technical Information Center
ATTN: C. MacDonald

SRI International
ATTN: *G. Abrahamson*
ATTN: A. Florence

Tetra Tech, Inc.
ATTN: Library
ATTN: L. Hwang

Weidlinger Assoc., Consulting Engineers
3 cy ATTN: M. Baron

Weidlinger Assoc., Consulting Engineers
ATTN: J. Isenberg